

RI 8988

<b>RI</b>	<b>8988</b>
-----------	-------------

PLEASE DO NOT REMOVE FROM LIBRARY

Bureau of Mines Report of Investigations/1985

# Electrical Ignition Energies and Thermal Autoignition Temperatures for Evaluating Explosion Hazards of Dusts

By Martin Hertzberg, Ronald S. Conti, and Kenneth L. Cashdollar



UNITED STATES DEPARTMENT OF THE INTERIOR



**Report of Investigations 8988**

# **Electrical Ignition Energies and Thermal Autoignition Temperatures for Evaluating Explosion Hazards of Dusts**

**By Martin Hertzberg, Ronald S. Conti, and Kenneth L. Cashdollar**



**UNITED STATES DEPARTMENT OF THE INTERIOR**  
Donald Paul Hodel, Secretary

**BUREAU OF MINES**  
Robert C. Horton, Director

Library of Congress Cataloging in Publication Data:

**Hertzberg, Martin**

Electrical ignition energies and thermal autoignition temperatures for evaluating explosion hazards of dusts.

(Report of investigations ; 8988)

Bibliography: p. 36-39.

Supt. of Docs. no.: I 28.23: 8988.

1. Mine explosions--Statistical methods. 2. Coal mines and mining--Pennsylvania--Dust control. I. Conti, R. S. (Ronald S.). II. Cashdollar, Kenneth L. III. Title. IV. Series: Report of investigations (United States. Bureau of Mines) ; 8988.

TN 23.U43 [TN 313] 622s [622'.334] 85-600119

## CONTENTS

	<u>Page</u>
Abstract.....	1
Introduction.....	2
Acknowledgments.....	4
Apparatus and experimental method.....	4
1.2-L furnace.....	4
8-L and 20-L chambers.....	7
Data.....	7
Properties of the dusts.....	7
Thermal autoignition data.....	9
Effective spark energies.....	11
Electrical ignitability data.....	16
Pittsburgh seam coal.....	16
Lycopodium.....	18
Modified Burgess-Wheeler law and lycopodium.....	19
Polyethylene.....	23
Discussion and analysis.....	26
Classification of electrical ignition hazards.....	27
Refinement of the theory of minimum ignition energies for gases.....	30
Conclusions.....	36
References.....	36
Appendix.--Symbols and nomenclature.....	40

## ILLUSTRATIONS

1. Example of domains of flammability and thermal autoignitability for coal dust in air.....	2
2. Vertical cross section of the 1.2-L furnace used to measure thermal and spark ignitability.....	5
3. Thermocouple traces of the temperature within the 1.2-L furnace during the dispersion of 130 g/m <sup>3</sup> of coal dust at increasing initial furnace temperatures .....	5
4. Schematic of electric spark ignition circuit and electrode configuration in the 1.2-L furnace.....	6
5. Thermocouple traces of the temperature within the 1.2-L furnace during the dispersion of 130 g/m <sup>3</sup> of coal dust at the same initial temperature of 500° C, but at two different spark energies.....	7
6. Vertical cross section of 20-L chamber used to measure spark ignitability	8
7. Horizontal cross section of 20-L chamber.....	8
8. Scanning electron microscope photographs of Pittsburgh coal dust, lycopodium, and polyethylene at two magnifications.....	9
9. Thermal autoignition data for minus 200-mesh Pittsburgh coal dust in the 1.2-L furnace.....	10
10. Thermal autoignition data for lycopodium.....	10
11. Thermal autoignition data for polyethylene.....	10
12. Effective spark energies as a function of capacitance for a test volume of 0.147 L at a charging potential of 300 V.....	14
13. Effective spark energies as a function of capacitance for a test volume of 0.379 L at a charging potential of 300 V.....	14
14. Effective spark energies as a function of stored electrical energy for several test volumes and charging potentials.....	15
15. Ignition and nonignition data points at an effective spark energy of 0.250 J for minus 200-mesh Pittsburgh coal in the 1.2-L furnace.....	16
16. Spark ignitability data for minus 200-mesh Pittsburgh coal in the 1.2-L furnace at various spark energies.....	16

ILLUSTRATIONS--Continued

	<u>Page</u>
17. Spark ignitability data for Pittsburgh coal in the 8-L and 20-L chambers compared with 1.2-L furnace data at room temperature.....	17
18. Ignition and nonignition data points at an effective spark energy of 0.050 J for lycopodium in the 1.2-L furnace.....	18
19. Spark ignitability data for lycopodium in the 1.2-L furnace at various spark energies.....	18
20. Spark ignition energy versus dust concentration for lycopodium in the 1.2-L furnace at room temperature and elevated temperatures.....	22
21. Temperature dependence of the lean flammability limit for lycopodium in air.....	23
22. Spark ignitability data for lycopodium in the 20-L chamber compared with 1.2-L furnace data at room temperature.....	24
23. Ignition and nonignition data points at an effective spark energy of 0.070 J for polyethylene in the 1.2-L furnace.....	24
24. Spark ignitability data for polyethylene at various spark energies in the 1.2-L furnace.....	25
25. Spark ignitability data for polyethylene in the 20-L chamber compared with 1.2-L furnace data at room temperature.....	26
26. Concentration dependence for the electrical ignitability of lycopodium at room temperature.....	27
27. Relationship between the minimum ignition energy and the quenching diameter for gases.....	35

TABLES

1. Properties of the three dusts.....	8
2. Summary of measured flammability and ignitability parameters for the three dusts.....	30

UNIT OF MEASURE ABBREVIATIONS USED IN THIS REPORT

atm	atmosphere	kcal/mol	kilocalorie per mol
°C	degree Celsius	kV	kilovolt
°C/min	degree Celsius per minute	L	liter
cal/g	calorie per gram	mil	milli-inch
cm	centimeter	mJ	millijoule
cm <sup>3</sup>	cubic centimeter	µm	micrometer
g/cm <sup>3</sup>	gram per cubic centimeter	ms	millisecond
g/m <sup>3</sup>	gram per cubic meter	pct	percent
J	joule	s	second
K	kelvin	V	volt

# ELECTRICAL IGNITION ENERGIES AND THERMAL AUTOIGNITION TEMPERATURES FOR EVALUATING EXPLOSION HAZARDS OF DUSTS

By Martin Hertzberg,<sup>1</sup> Ronald S. Conti,<sup>2</sup> and Kenneth L. Cashdollar<sup>3</sup>

---

## ABSTRACT

The Bureau of Mines measured the energy requirements for the spark ignition in air of Pittsburgh seam bituminous coal dust, lycopodium spores, and polyethylene powder with a 1.2-L furnace and 8-L and 20-L chambers. Thermal autoignition temperatures of the same dusts were measured in the 1.2-L furnace. Electrical ignition requirements are given in terms of both effective spark gap energies,  $\epsilon_{eff}$ , and stored circuit energies,  $1/2 CE^2$ .

The measured order of electrical ignitability for the three dusts is consistent with the data of other researchers; however, the absolute values are systematically higher, probably because of higher flow and turbulence levels in the chambers used and lower electrical efficiency in the circuit used here.

The temperature dependence of the lean limit of flammability for lycopodium was measured with the 1.2-L system, and those measurements confirm the applicability of the modified Burgess-Wheeler law to a dust.

Due to experimental complexities, the minimum ignition energies for dusts may not reflect intrinsic flammability behavior. However, some valuable information may be obtained from the relative ignition energies of various dusts at ambient and elevated temperatures. In addition, the concept of minimum electrical ignition energies for homogeneous gas mixtures is reevaluated theoretically.

---

<sup>1</sup>Supervisory research chemist.

<sup>2</sup>Electronics engineer.

<sup>3</sup>Physicist.

Pittsburgh Research Center, Bureau of Mines, Pittsburgh, PA.

## INTRODUCTION

The probability of the occurrence of a fuel-air explosion in any given region of space is the product of the probabilities of two conditions that are usually mutually independent of one another. The first is the existence of a flammable volume within that space, to which is ascribed a probability,  $Pr(f)$ . The second is the presence of an ignition source of sufficient intensity to initiate a combustion wave within that volume, and its probability is  $Pr(i)$ . The net explosion probability,  $Pr(expl) = Pr(f)Pr(i)$ , is the product of these two probabilities. Thus, while an accurate knowledge of the limits of flammability of a substance is an essential ingredient in quantifying the first of these probabilities (11, 25-26, 47),<sup>4</sup> the ignition probability can be of comparable importance in obtaining a realistic appraisal of the total explosion hazard involved in the mining, manufacturing, transportation, storage, and use of that substance. Such safety concerns have motivated numerous experimental and theoretical studies of the energies required for spark ignition and the temperatures required for thermal ignition of both gases and dusts (5, 18, 26, 28, 33, 37, 39, 48).

The ignition parameters that are generally measured are the minimum autoignition temperature (AIT) and the minimum spark ignition energy. Those parameters are essential for estimating the probability of thermal ignition,  $Pr(i,t)$ , or the probability of electrical ignition,  $Pr(i,spark)$ , in any given physical system. This report will present the data obtained for both the thermal and electrical ignition probability for three dusts: Pittsburgh seam bituminous coal, lycopodium, and polyethylene. Also to be considered is the theoretical problem of predicting spark ignition energies for both gases and dusts. Finally, this report contains a consideration of the spark ignitability parameters that are

most appropriate to use in assessing practical explosion hazards.

Before the data are presented and discussed, it is important to consider the format and context in which the ignitability data will be presented. That format, an example of which is shown in figure 1, helps to clearly distinguish the differences between the aforementioned probabilities: the first probability dealing with the existence of a flammable volume, and the second dealing with the main subject of this report, i.e., the probability of the ignition of that flammable volume. The relationship will be considered generally in the form of a thermodynamic abstraction and then in

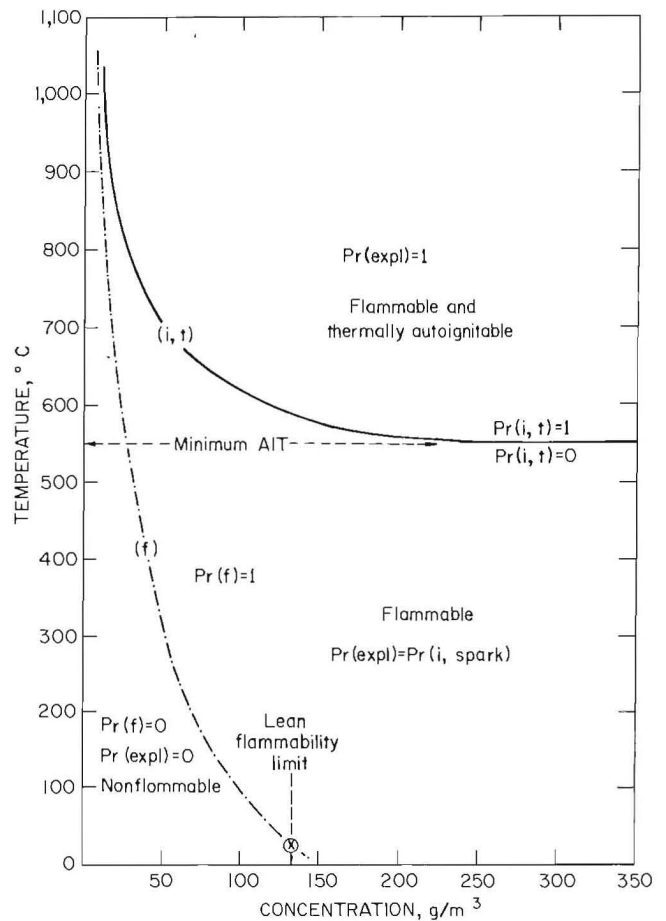


FIGURE 1. - Example of domains of flammability and thermal autoignitability for coal dust in air at 1 atm. Solid line (i,t) is the thermal autoignitability limit, and dot-dashed line (f) is the flammability limit.

<sup>4</sup>Underlined numbers in parentheses refer to items in the list of references preceding the appendix.

concrete terms using the specific example shown in figure 1.

The abstraction to be used is the classical one of thermodynamic state-space (16). The domain of all thermodynamic states available to any uniform mixture of fuel in air is describable by an  $n$ -dimensional space whose independent variables are the initial temperature,  $T$ , the initial pressure,  $p$ , and the initial composition variables such as the mol fractions ( $x_i$ 's). The flammability range of any uniform mixture is describable as some limiting surface in that thermodynamic state-space. That surface or discontinuity separates a domain of flame propagation within it from a region outside it where flame propagation is not possible. Thus, on the inside of the surface  $\text{Pr}(f) = 1$ , whereas on the outside of the surface  $\text{Pr}(f) = 0$ . That mathematical surface is the flammability limit surface which describes a real discontinuity in the combustion behavior of any system in its earthly environment. The thermodynamic states on the outside of the discontinuity are "nonflammable" or "nonexplosive."

For example, consider the usual description of lean (lower) and rich (upper) limits of flammability at room temperature and atmospheric pressure. It should be recognized that those composition limits are merely two points on the flammability limit surface. The isobaric plane at  $p = 1$  atm and the isothermal plane at  $T = 25^\circ \text{C}$  intersect in a line. The intersection of that line with the flammability limit surface defines those two points: the one is the lean limit at room temperature and atmospheric pressure, and the other is the rich limit at that same temperature and pressure. Clearly, there are many other important "points" or "curves" on the surface or boundary that defines the domain of flammable thermodynamic states. A given mixture that is nonflammable at atmospheric pressure can become flammable at an elevated pressure. The total pressure at which such a mixture becomes flammable is thus also a limit of flammability. Similarly, a mixture that is nonflammable at some low initial temperature may become flammable at an elevated temperature.

That too is a limit of flammability. Finally, consider the temperature dependences of the lean or rich limit compositions: those are important "curves" on the flammability limit surface.

A concrete example is shown in figure 1, which is the temperature versus dust concentration cross section from the thermodynamic state-space of the system taken at the constant pressure plane of 1 atm for fine Pittsburgh seam coal dust in air. Curve (f) is the best estimate of the intersection of the flammability limit surface with the 1-atm constant pressure plane. To the left and below it, the dust is nonflammable and  $\text{Pr}(f) = 0$ ; to the right and above it,  $\text{Pr}(f) = 1$ . That dot-dashed contour is drawn from the measured datum point at  $25^\circ \text{C}$ . It is extended to elevated temperatures according to the modified Burgess-Wheeler law (47). For all states of the system below and to the left of that contour, the explosion probability  $\text{Pr}(\text{expl}) = 0$  because the probability of a flammable volume  $\text{Pr}(f) = 0$ . Above and to the right of that contour the mixtures are all flammable and the explosion probability becomes equal to the ignition probability; that is,  $\text{Pr}(\text{expl}) = \text{Pr}(f)\text{Pr}(i) = \text{Pr}(i)$ .

It should be clearly understood that the precondition for determining whether propagation can occur in a system is the requirement that a combustion wave be present initially. Thus the ignition source used to measure whether or not a given thermodynamic state is flammable must always be strong enough to initiate the normal combustion wave. That wave must first exist before one can test whether it is capable of propagating freely into the medium under study. In practice, that condition is satisfied most simply by increasing the energy of the ignition source until the measured limit of flammability is independent of the strength of the ignition source. Thus, the true flammability limit surface corresponds, conceptually, to the propagation discontinuity measured with an essentially unlimited ignition energy in a system of infinite volume. Curve (f) represents a constant pressure contour on that surface.

The upper curve in figure 1 labeled (i,t) is the thermal autoignition curve measured at ambient pressure in a constant-temperature furnace (9). The data obtained to delineate that curve will be presented later. All regions above and to the right of that upper curve are regions where the explosion probability  $Pr(\text{expl}) = 1$ . Explosion is certain in that region of state-space because the probability of the existence of a flammable volume,  $Pr(f)$ , and the probability of thermal autoignition,  $Pr(i,t)$ , are both unity.

In the region between the two curves, although the mixtures are flammable, they are not thermally autoignitable. However, if any external energy source is simultaneously present while the system is in that intermediate region of state-space, then the explosion probability becomes equal to the ignition probability from that external source. The specific external ignition source to be considered in this report is the electric spark, and data will be presented for this intermediate zone in which  $Pr(\text{expl}) = Pr(i, \text{spark})$ . The spark ignitability domains will be delineated in this intermediate zone as a function of spark energy.

Clearly, fuels that are easily ignited by electric sparks will be characterized by ignitability curves that lie close to the lower curve (f), so that their ignitability domain includes a large portion of the intermediate zone. However, curves for fuels that are difficult to ignite by electric sparks will have ignitability curves that tend to approach the upper curve (i,t), so that ignitability domain includes only a small fraction of the intermediate zone.

The two quantities that conveniently describe the main flammability and thermal autoignitability characteristics for any dust mixture are defined in figure 1. The one is the lean flammability limit at room temperature, which is sometimes referred to as the minimum explosive concentration. The other is the minimum autoignition temperature (AIT), which is sometimes referred to as the minimum cloud ignition temperature. The minimum AIT is usually approached only at high dust concentrations. The data to be presented in this report are the spark ignitability curves, to be delineated in the intermediate region between the upper and lower curves as a function of the effective energy of the spark.

#### ACKNOWLEDGMENTS

The authors wish to thank L. Welsch and J. Verscharen (physical science aids) for their assistance in the collection of the data for this report and F. Duda (electrical engineer) for his assistance in the development of the instrumentation.

They also wish to thank Y. Miron (chemical engineer) for obtaining the differential thermal analysis data for polyethylene. All concerned are personnel of the Pittsburgh Research Center, Bureau of Mines.

#### APPARATUS AND EXPERIMENTAL METHOD

##### 1.2-L FURNACE

The majority of the thermal autoignition and spark ignition data to be reported here were obtained with a 1.2-L furnace. Additional spark ignition data were obtained in 8-L and 20-L chambers. The furnace and its dust dispersion system were described in detail in an earlier report (10). A schematic of the 1.2-L furnace and the dust dispersion receptacle are shown in figure 2. In normal

operation, a glass, microfiber filter diaphragm is placed in a holder on the top of the furnace. The dust to be tested is placed in the dispersion receptacle, which is inserted quickly into the bottom of the furnace. A 30-ms air pulse that sends about 100 cm<sup>3</sup> of air from the dispersion tank into the furnace generates a fairly uniform dust cloud in the furnace. The earlier report presented data on the uniformity of the temperature distribution within the furnace volume and the

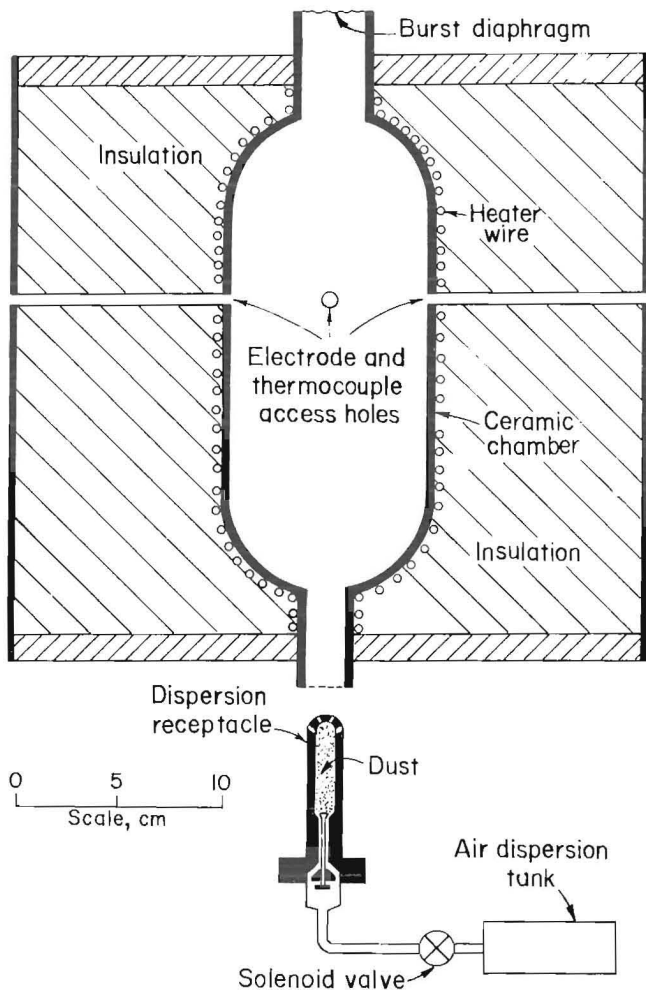


FIGURE 2. - Vertical cross section of the 1.2-L furnace used to measure thermal and spark ignitability.

homogeneity of the dust dispersion. Also described were the criteria used to decide whether the test mixture was thermally ignitable under a given set of initial conditions. The same criteria (rupture of the diaphragm at the top of the furnace and flame emitting outward) were used to decide whether a test mixture was electrically ignitable. As indicated in figure 2, four additional access holes pass into the 1.2-L furnace. Two of those holes are used for thermocouples. One, a 12.5-mil (318- $\mu\text{m}$ ) Chromel-Alumel<sup>5</sup> thermocouple, is located at the wall of the furnace and is used to control the

<sup>5</sup>Reference to specific products does not imply endorsement by the Bureau of Mines.

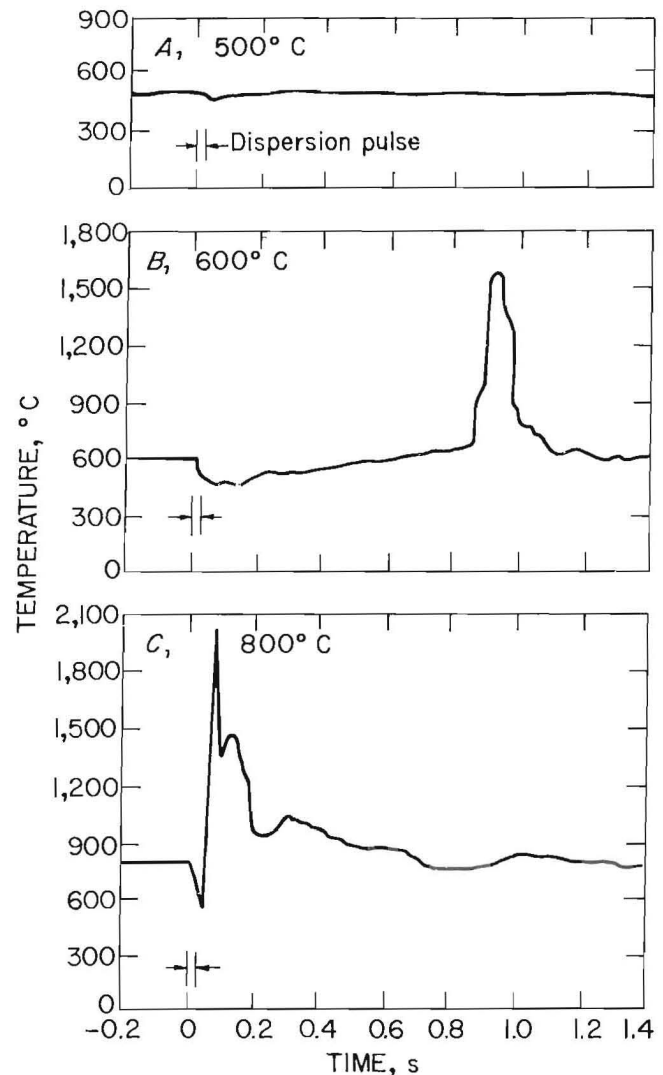


FIGURE 3. - Thermocouple traces of the temperature within the 1.2-L furnace during the dispersion of 130 g/m<sup>3</sup> of coal dust at increasing initial furnace temperatures.

furnace temperature. The other, a 1-mil (25- $\mu\text{m}$ ) platinum-rhodium thermocouple, is positioned near the center of the furnace and is used to measure the rapid changes in the temperature of the dust-air mixture at ignition.

Some examples of the thermal ignitability data are shown in figure 3. Figure 3A is the temperature trace measured with the 1-mil thermocouple for a dust concentration of 130 g/m<sup>3</sup> of Pittsburgh seam pulverized coal dispersed through the bottom into the furnace. Reference to figure 1 shows that while 130 g/m<sup>3</sup> at  $T = 500^\circ\text{C}$  is in the flammable domain, it

is not thermally autoignitable. Thus, there is no ignition, the measured temperature remains relatively constant, and no explosion is observed. Figure 3B is the 1-mil thermocouple trace for the same dust concentration of  $130 \text{ g/m}^3$  but at the higher temperature of  $600^\circ \text{ C}$ . Reference to figure 1 shows that that point in concentration-temperature space is just above the thermal ignitability curve so that it is in a region that is both flammable and thermally autoignitable. The thermocouple trace in figure 3B shows this quite clearly. There is initially a small drop in temperature as the dust and air at room temperature are dispersed into the hot furnace. The temperature soon returns to the set temperature of the furnace, and at 0.9 s after the dispersion pulse there is a rapid increase in temperature, indicating autoignition of the dust. The explosion ruptures the diaphragm at the top of the furnace, and flame is emitted from the vented top. The final trace, figure 3C, is for the same dust concentration of  $130 \text{ g/m}^3$  but at an even higher initial furnace temperature of  $800^\circ \text{ C}$ . That combination of concentration and temperature is well within the domain where the explosion probability is unity. The thermocouple trace in figure 3C shows the same initial cooling as the cold dust and air are injected into the furnace. In this case, however, thermal autoignition occurs even before the mixture reaches the initial furnace temperature. Since the furnace temperature substantially exceeds the autoignition temperature, the ignition in figure 3C occurs at virtually the instant the dust is dispersed. In this case the propagation rate is very rapid and the thermocouple measures a burned-gas temperature of over  $2,000^\circ \text{ C}$  just before those gases vent through the burst diaphragm. The vented system quickly cools down to the oven temperature.

For measurements of the electrical ignition probability at various energies, the two additional access holes were used for spark electrodes. The electrodes were located near the center of the furnace, as shown in figure 4. Details of the electrode spacing and the circuit

used to store the electrical energy to be deposited into the spark are described in the "Effective Spark Energies" section. A simplified version of that circuit is also shown in figure 4. A capacitor of capacitance  $C$  is charged to a potential  $E$  and then discharged through a high-voltage, step-up transformer, producing a spark at the electrode gap in the furnace. The stored electrical energy is  $1/2 CE^2$ , and the fraction that is deposited into the gas is measured independently, as described in the "Effective Spark Energies" section.

Examples of the thermocouple temperature measurements made during the spark ignitability tests are shown in figure 5. In both cases the coal dust concentration

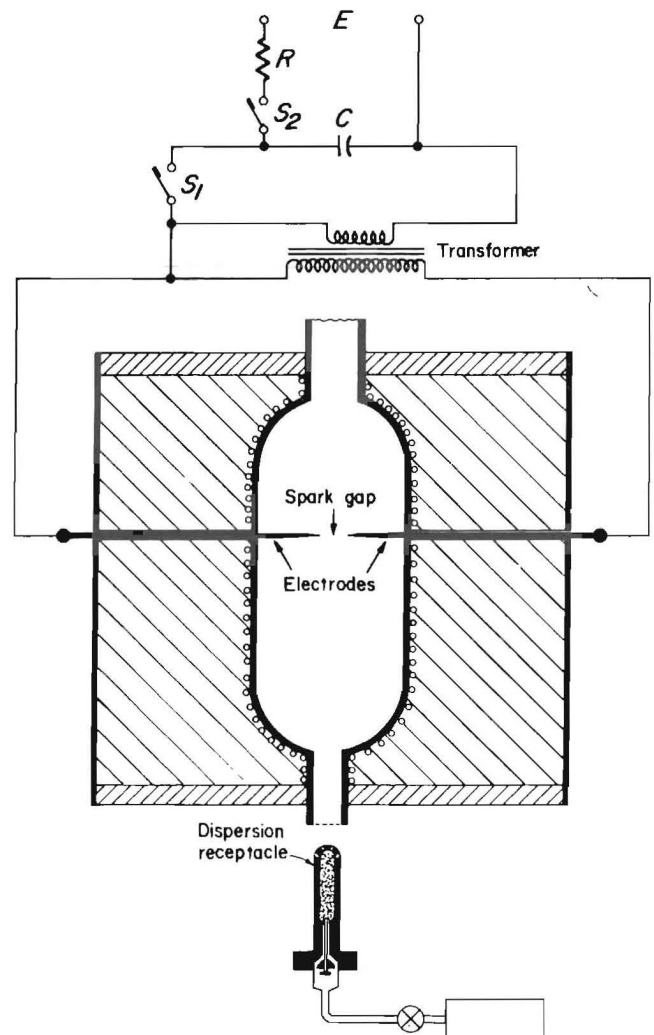


FIGURE 4. - Schematic of electric spark ignition circuit and electrode configuration in the 1.2-L furnace.

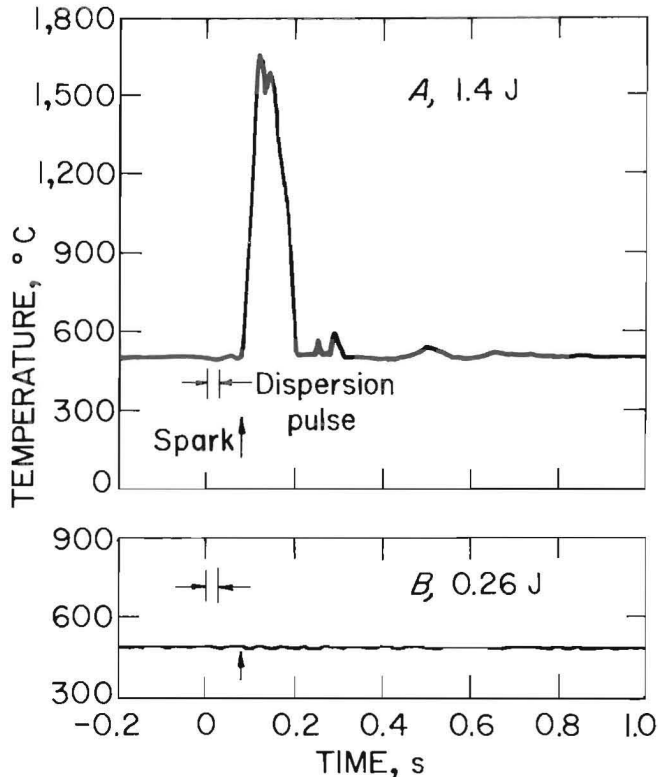


FIGURE 5. - Thermocouple traces of the temperature within the 1.2-L furnace during the dispersion of  $130 \text{ g/m}^3$  of coal dust at the same initial temperature of  $500^\circ \text{C}$ , but at two different spark energies.

was  $130 \text{ g/m}^3$  and the initial furnace temperature was  $500^\circ \text{C}$ . The temperature trace observed for that combination of dust concentration and temperature in the absence of a spark has already been shown in figure 3A. That combination is not thermally autoignitable. However, the trace in figure 5A shows that an explosion occurs in the presence of a spark whose effective energy (to be defined later) is about 1.4 J.

The data in figure 5B are for the same concentration and temperature but for a lower effective spark energy of 0.26 J. There is no explosion and the trace is essentially similar to that in figure 3A

because the ignition energy is now insufficient to ignite the mixture even though it is flammable.

#### 8-L AND 20-L CHAMBERS

Spark ignitability data at room temperature were also obtained in 8-L and 20-L chambers. These systems, which were routinely used for measuring flammability limits for dusts, were fitted with spark electrodes attached to an electrical ignition circuit similar to that shown in figure 4. The details of the design and operation of the 8-L chamber have already been described in detail (25, 27).

The 20-L chamber is an improved version of the 8-L chamber and is shown in figures 6 and 7. Optical dust probes (8, 10, 27, 34) are used to measure the dust dispersion uniformity. Six bolts secure the hinged top, which can be opened easily to load the dust (by unscrewing the dispersion nozzle) into the reservoir. The chamber is preevacuated to 0.14 atm absolute, and the dust is dispersed by a 0.3-s blast of air at 14 atm. This dispersion air ejects the dust through the nozzle and disperses it throughout the chamber while raising the pressure back to 1 atm absolute. The spark electrodes are located near the center of the chamber (shown as the ignition point on the figures), and the spark is energized at 0.1 to 0.5 s after the end of the air dispersion pulse. The pressure transducer measures the resulting explosion pressure. The criterion for ignition is a pressure ratio (maximum explosion pressure divided by pressure at ignition) of 2 or, equivalently, a pressure rise of about 1 atm. The oxygen sensor in figure 7 can be used to measure the residual oxygen content in the chamber after the explosion.

#### DATA

##### PROPERTIES OF THE DUSTS

The properties of the three dusts whose electrical ignitability properties were studied are given in table 1 in order of

increasing volatility. The surface and mass mean diameters,  $\bar{D}_s$  and  $\bar{D}_w$ , were calculated from Coulter counter (4) particle size analyses. The proximate and ultimate analyses and the heating values

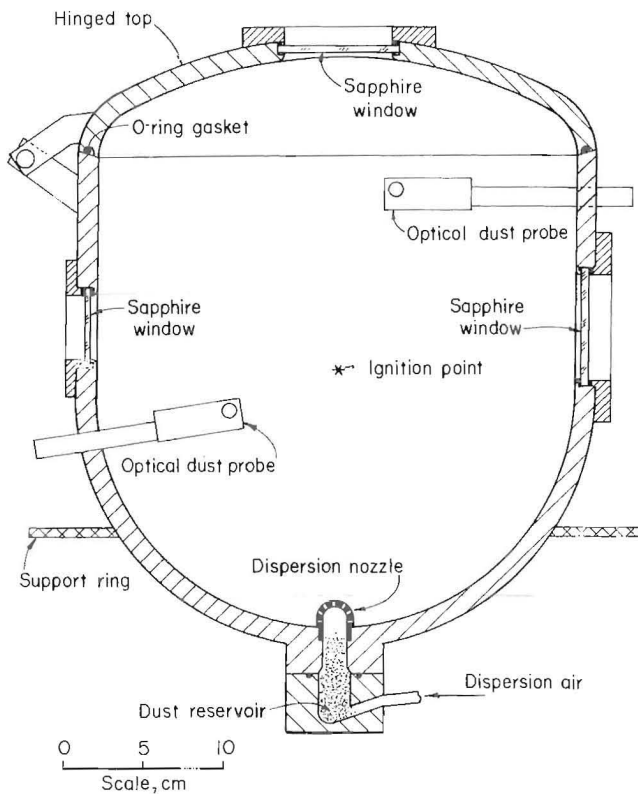


FIGURE 6. - Vertical cross section of 20-L chamber used to measure spark ignitability.

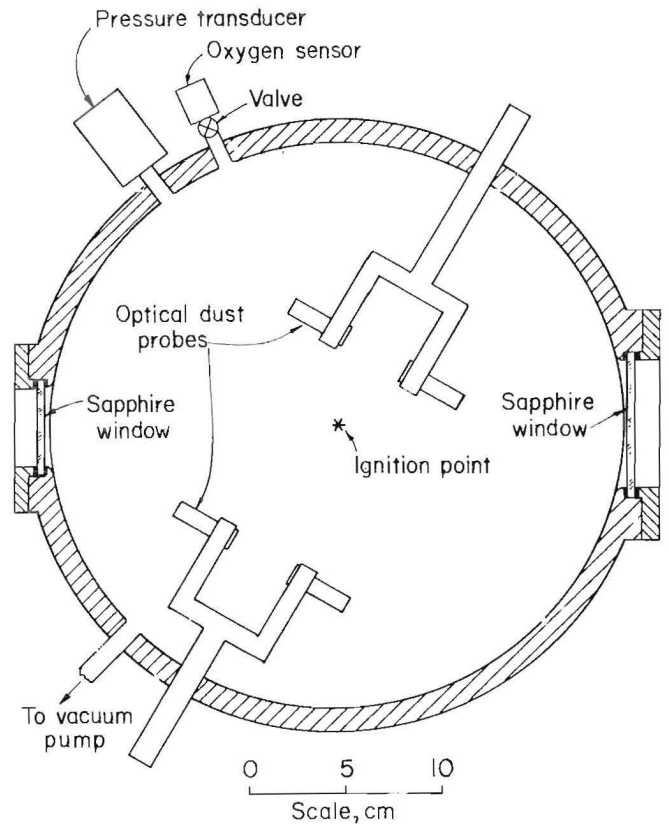


FIGURE 7. - Horizontal cross section of 20-L chamber.

TABLE 1. - Properties of the three dusts

	Pittsburgh coal	Lycopodium	Polyethylene
Mean diameter, $\mu\text{m}$ :			
$\bar{D}_s$ .....	23	27	26
$\bar{D}_w$ .....	31	28	31
Proximate analysis, pct:			
Volatiles.....	37.0	85.2	99.5
Moisture.....	0.5	1.8	0.0
Fixed carbon.....	57.2	11.6	0.4
Ash.....	5.3	1.4	0.1
Ultimate analysis (ash-free), pct:			
C.....	82.9	67.7	85.5
H.....	5.5	9.7	14.1
N.....	1.6	1.4	0.1
O.....	8.9	21.0	0.3
S.....	1.3	0.1	0.0
H:C ratio.....	0.80	1.72	1.98
Heating value, cal/g:			
Total.....	7,830	7,400	11,090
Volatile.....	2,900	6,310	11,030
Density.....g/cm <sup>3</sup> ..	1.3	0.8	0.9

were obtained using standard test methods (1, 45).

The first column is minus 200-mesh Pittsburgh seam bituminous coal, which is 37 pct volatile and has the lowest H:C ratio (0.80) of the three dusts. Lycopodium powder is a naturally occurring plant spore with an H:C ratio of 1.72. It contains a substantial amount of oxygen atoms in its structure together with a small amount of nitrogen. Some 85 pct of the lycopodium mass volatilizes upon pyrolysis, leaving a char ("fixed carbon") and ash residue of only about 13 pct of its original mass. The third column is the almost completely volatilizable polyethylene. It is a saturated, aliphatic hydrocarbon with an empirical formula of  $(CH_2)_n$  and an H:C ratio of 1.98. It contains no aromatic structures, almost no "fixed carbon" residue after pyrolysis, and no ash, oxygen, sulfur, or nitrogen.

Figure 8 shows scanning electron microscope photographs of the three dusts in their original, unreacted condition. The lycopodium structure is the most interesting one, as can be seen in figures 8C and 8D. It has a remarkably uniform particle diameter of about 27  $\mu\text{m}$ . Its shape and porous outer structure reveal its natural origin. The porous structure gives a particle density of approximately 0.8  $\text{g}/\text{cm}^3$ . The polyethylene in figures 8E and 8F shows a range of sizes; the individual particles are usually rounded. The coal dust used is shown in figures 8A and 8B; the particles have a range of sizes and sharp edges and corners.

#### THERMAL AUTOIGNITION DATA

Before presenting the data on spark ignition, it is necessary to accurately define the intermediate domain of initial temperatures and concentrations within which these measurements are made. That intermediate domain corresponds to mixtures that are flammable but not thermally autoignitable. As indicated in the introduction, it is the domain in figure 1 between the curve (f) and the curve (i,t) within which the explosion probability,  $\text{Pr}(\text{expl})$ , is equal to the spark ignition probability,  $\text{Pr}(i,\text{spark})$ . In

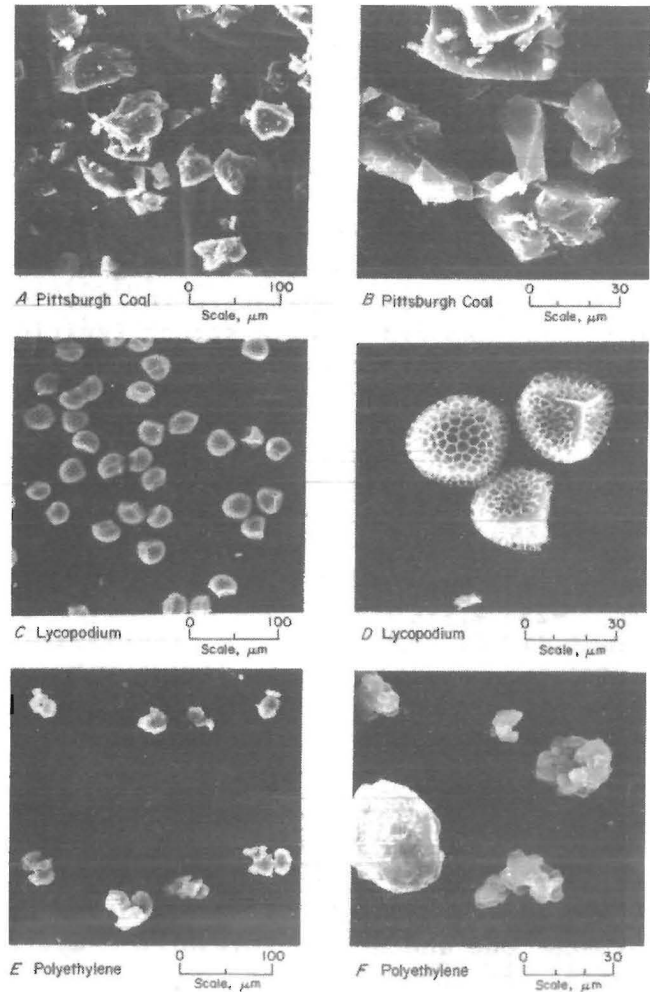


FIGURE 8. Scanning electron microscope photographs of Pittsburgh coal dust, lycopodium, and polyethylene at two magnifications.

this section, the data from the 1.2-L furnace used to delineate the thermal autoignition curve (i,t) will be presented for the three dusts listed in table 1.

The autoignition data for minus 200-mesh Pittsburgh seam bituminous coal ( $\bar{D}_s = 23 \mu\text{m}$ ) are shown in figure 9. The minimum autoignition temperature is near 560° C. That value is significantly higher than the values for the other two dusts; therefore the coal is more difficult to ignite thermally. It is less ignitable because of its lower volatility and its lower rate of devolatilization in the temperature ranges of interest. All concentrations above the thermal autoignition curve (solid line) ignite spontaneously. Concentrations below that curve

do not ignite spontaneously even though they may be flammable.

The lean flammability limit is also shown as the dot-dashed curve in figure 9. It is extrapolated from the lean flammability limit datum point at 25° C to elevated temperatures according to the modified Burgess-Wheeler (B-W) law. That lean limit datum point of 130 g/m<sup>3</sup> was measured at room temperature in the 8-L and 20-L chambers using a strong ignition source of four chemical matches (25, 27).

The B-W law will be derived in detail in a subsequent section. Here the empirical B-W law for dusts is given without derivation as

$$C_T = C_{25} \left[ \frac{298}{T+273} \right] [1 - 0.000721 (T-T_0)], \quad (1)$$

where  $C_T$  is the lean flammability limit at any temperature  $T$  (in degrees Celsius) and  $C_{25}$  is the lean flammability limit at room temperature,  $T_0 = 25^\circ \text{C}$ . As can be seen from figure 9, the lean flammability limit and thermal autoignition curves approach one another at elevated temperatures. At those elevated temperatures it would appear that all flammable mixtures are also spontaneously autoignitable.

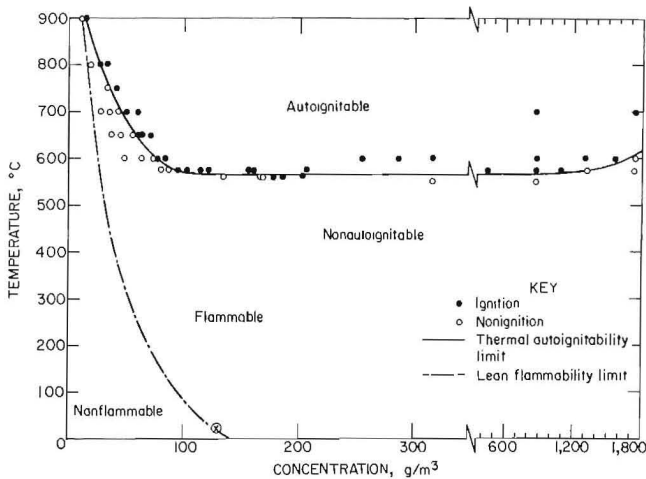


FIGURE 9. - Thermal autoignition data for minus 200-mesh Pittsburgh coal dust in the 1.2-L furnace.

Also shown in figure 9 are some autoignition data at very high coal dust concentrations. There is very little upward curvature until concentrations exceed 1,500 g/m<sup>3</sup>. The upward curvature may be suggestive of the eventual existence of a rich limit of flammability at much higher dust concentrations.

The autoignition data for lycopodium powder are shown in figure 10. The minimum autoignition temperature, which is approached asymptotically at high dust concentrations, is 420° C. A lean flammability limit curve based on the B-W law extrapolated from the lean flammability limit measurement at room temperature in the 20-L chamber is also shown.

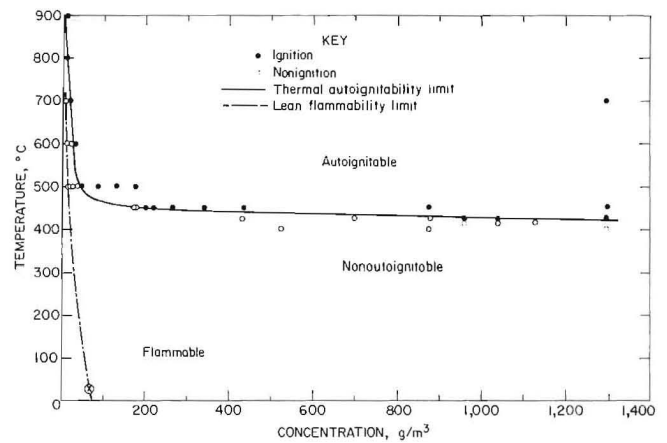


FIGURE 10. - Thermal autoignition data for lycopodium.

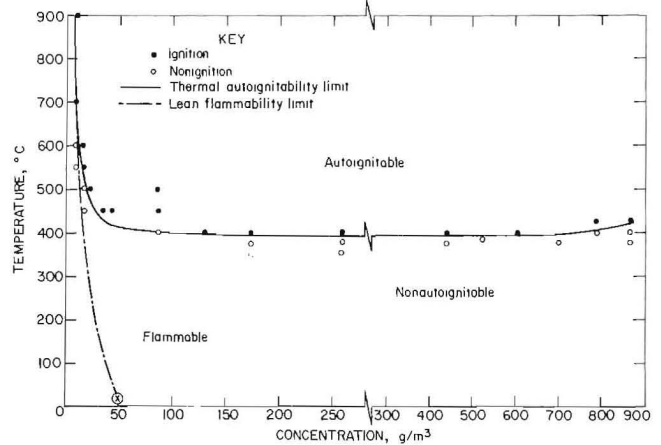


FIGURE 11. - Thermal autoignition data for polyethylene.

The autoignition data for the  $\bar{D}_s = 26$   $\mu\text{m}$  polyethylene are presented in figure 11. The minimum autoignition temperature is estimated to be about  $395^\circ\text{C}$ . The solid upper curve is the thermal autoignition curve. All concentrations and temperatures above and to the right ignite spontaneously. The concentrations below that curve do not ignite spontaneously even though they may be flammable. The dot-dashed curve is the flammability limit curve extrapolated from the room temperature datum point of  $45 \pm 5 \text{ g/m}^3$ , which is the lean flammability limit concentration for polyethylene in air at ambient temperature measured in the 8-L chamber (25) using a four-match ignitor.

It is interesting to compare the heating values in table 1 with the minimum AIT's for the three dusts. Coal's total heating value in table 1 is less than that of polyethylene but similar to that of lycopodium; however, that total heating value is somewhat misleading. The coal's total heating value includes contributions from both the volatiles and the char, whereas in reality the char makes no significant contribution to the reaction exothermicity on the time scale required for ignition and flame propagation in explosions. The heating values of both the coal and lycopodium are also calculated on the basis of the volatiles' contributions in table 1. On that basis, the coal heating value is much less than that for lycopodium. The coal is the most difficult to ignite because the effective exothermicity of its volatiles per unit mass of dust is also the lowest. The measured AIT's vary consistently with the respective volatile heating values for all three dusts.

#### EFFECTIVE SPARK ENERGIES

With the thermal autoignitability and flammability curves delineated in figures 9, 10, and 11, it is possible to measure the spark ignitability in the intermediate domain. As indicated earlier, the intermediate domain corresponds to states of the system that are flammable but not thermally autoignitable. In the presence of an external ignition source such as a

spark, the explosion probability in this region is equal to the ignition probability. Thus, in the intermediate domain, in the presence of a spark ignition source, the presence or absence of a measured explosion can be directly attributable to that ignition source and its energy level or strength. Before the spark ignition data can be presented in a meaningful way, it is first necessary to measure and control the strength of that external electrical source.

The following derivation defines that quantity, the effective spark energy,  $\epsilon_{\text{eff}}$ . It is the energy available to initiate the combustion process in a test mixture whose electrical ignitability is to be measured. Note that, for reference, all of the algebraic symbols used are defined in the appendix.

Electrical energy, stored in that external circuit, is deposited into that spark gap in the form of an electron-ion avalanche discharge. The discharge occurs when the high voltage applied between the electrodes generates an electric field of sufficient intensity to break down the gas mixture in the gap and cause it to conduct. While it is relatively easy to measure the stored electrical energy, it is much more difficult to measure or control the fraction of that energy that is really available to initiate the combustion process in the test mixture.

Consider a small, initial channel volume,  $v_1$ , through which an electrical discharge is to pass. The channel volume is typically of cylindrical shape between two spark electrodes. It is initially at ambient temperature,  $T_0$ , but when the spark is discharged through the electrodes, that channel volume is heated to some elevated temperature  $T_f$  as a result of the deposition of energy,  $E_1$ , from the external electrical circuit. The heating of that volume results in its expansion to a larger volume,  $v_f$ . Since no mass is added by the deposited spark energy,  $E_1$ , and since the typical time constant for the discharge of energy in the electron-avalanche process is much shorter than the time required for the thermal energy dissipation process between the channel

volume and its surroundings, it is assumed that the final volume of the heated channel can be obtained from the initial volume by the ideal gas law. If the dissociated and ionized fraction in the final discharge volume is small, the average molecular weight remains unchanged, and

$$v_f = v_i \frac{(T_f + 273)}{(T_o + 273)}. \quad (2)$$

Now the spark electrodes are located within a test chamber whose total initial volume is large and fixed at  $V_o$ . The initial channel volume,  $v_i$ , and the final spark channel volume,  $v_f$ , are both much smaller than the total test chamber volume,  $V_o$ . That total test chamber volume is composed of the spark volume and a surrounding, "unaffected" volume,  $V_u$ . Since  $V_o$  is constant,

$$V_o = (V_u)_i + v_i = (V_u)_f + v_f, \quad (3)$$

where  $(V_u)_i$  is the "unaffected" initial volume and  $(V_u)_f$  is the "unaffected" final volume. Naturally, the expansion of the spark volume from  $v_i$  to  $v_f$  results in a small pressure rise,  $\Delta p$ , within the test chamber volume. Thus the surrounding volume,  $(V_u)_i$ , is not completely "unaffected" because that small pressure rise results in its compression into a somewhat smaller volume,  $(V_u)_f$ . However, since  $v_f \ll V_o$ , the pressure rise  $\Delta p$  is very small compared to the initial ambient pressure  $p_o$ ; that is,  $\Delta p \ll p_o$ .

Now the deposited spark energy,  $E_i$ , appears in at least two forms: as thermal energy within the final spark volume,  $v_f$ , and also as the work of compression of the "unaffected" or surrounding volume,  $(V_u)_i$ . For the moment, it will be assumed that the energy lost by radiation and by the possible shock wave from the spark volume is small compared to the thermal energy and the work of compression. Thus

$$E_i = \epsilon_{eff} + w, \quad (4)$$

where  $\epsilon_{eff}$  is the thermal energy within the spark volume and  $w$  is the work done by that spark volume as it expands and compresses its surroundings. By using a thin paper test object suspended close to the spark volume, Eckhoff and Enstad were able to demonstrate the reality of the pressure force generated by the spark volume expansion (13-14). The measured deflection of such a ballistic pendulum is a direct reflection of the pressure force which compresses the surrounding volume. That work of compression is, however, so diluted throughout that surrounding volume,  $V_u$ , that the temperature rise in the surroundings is trivial. It is only the thermal energy within the spark volume that is sufficiently concentrated to ignite the test mixture, and accordingly that thermal energy is also defined as the effective spark energy,  $\epsilon_{eff}$ . The work portion,  $w$ , is incapable of igniting the mixture, but it does generate a measurable pressure rise,  $\Delta p$ . That work of compression is equal to the work done by the spark volume in expanding from  $v_i$  to  $v_f$ , and since  $\Delta p \ll p_o$ , that work is essentially isobaric. Thus

$$E_i = \int_{T_o}^{T_f} c(T) dT + p_o (v_f - v_i), \quad (5)$$

where  $c(T)$  is the heat capacity of the ignition volume in the spark channel and the integral is taken from its initial temperature,  $T_o$ , to its final temperature,  $T_f$ .

$$\begin{aligned} \text{Now let } \int_{T_o}^{T_f} c(T) dT &= \bar{c}(T_f - T_o) \\ &= \frac{\nu}{2} R (T_f - T_o), \quad (6) \end{aligned}$$

where the quantity  $\bar{c}$  is some effective heat capacity that is proportional to the gas constant,  $R$ , with a proportionality constant  $\nu/2$ . The quantity  $\nu$  is the

number of the degrees of freedom (translational, rotational, and vibrational) available to the atoms or molecules within the spark volume. Substituting equations 2 and 6 into equation 5 gives

$$E_f = \frac{v}{2} \frac{R(T_o + 273)}{v_f} (v_f - v_f) + p_o (v_f - v_f). \quad (7)$$

According to the ideal gas law,  $p_o = \frac{R(T_o + 273)}{v_f}$ , where the volumes are expressed per unit mol. Hence,

$$E_f = \left(\frac{v}{2} + 1\right) p_o (v_f - v_f). \quad (8)$$

From equation 3

$$v_f - v_f = \Delta v = - [(V_u)_f - (V_u)_f] = -\Delta V_u.$$

Now from the ideal gas law,

$$V = \frac{R(T + 273)}{p} \text{ and under isothermal conditions,}$$

$$\Delta V = - \frac{R(T + 273)}{p^2} \Delta p. \quad (9)$$

For the "unaffected" surroundings, the compression is approximately isothermal and hence

$$-(\Delta V_u) \approx \frac{R(T_o + 273)}{p_o^2} \Delta p \approx v_f - v_f. \quad (10)$$

Substituting equation 10 into equation 8 gives

$$E_f = \left(\frac{v}{2} + 1\right) \frac{R}{p_o} (T_o + 273) \Delta p = \left(\frac{v}{2} + 1\right) V_o \Delta p. \quad (11)$$

It should be noted from the derivation that

$$E_f = \epsilon_{eff} + w = \epsilon_{eff} + V_o \Delta p.$$

$$\text{Thus } \epsilon_{eff} = E_f - V_o \Delta p = \left(\frac{v}{2}\right) V_o \Delta p. \quad (12)$$

For a monatomic gas  $v = 3$  and

$$\epsilon_{eff} = 1.5 V_o \Delta p. \quad (13)$$

For a diatomic gas  $v = 5$  and

$$\epsilon_{eff} = 2.5 V_o \Delta p. \quad (14)$$

In several earlier ignition studies, the  $V_o \Delta p$  parameter was used to measure the strength of various ignition sources. One source that was convenient for dusts that are very difficult to ignite was a pyrotechnic or chemical match, and data were reported for arrays of such matches (25, 27). The chemical match differs from the spark because it also results in the addition of mass into the test volume,  $V_o$ , and the energy added is not as confined in space as for the spark. Accordingly, if mass is added, as with an electric match,  $\epsilon_{eff}$  may be a different multiple of the measured  $V_o \Delta p$  factor than is indicated in equation 14. For electric sparks in air, there is no mass addition, and equation 14 should be applicable since air is predominantly a diatomic gaseous medium.

The data obtained for two test volumes are shown in figures 12 and 13. The measured effective spark energies,  $\epsilon_{eff} = 2.5 V_o \Delta p$ , are plotted as a function of capacitance for three spark gap distances. Figure 12 is for a test volume of  $V_o = 0.147$  L, and figure 13 is for  $V_o = 0.379$  L. The data in both figures are for an input voltage of  $E = 300$  V discharged through a high-voltage transformer (rated at 15-kV output for 277-V ac input). The data show that for a given stored electrical energy,  $1/2 CE^2$ , the effective spark energy,  $\epsilon_{eff}$ , increases almost linearly with increasing gap distance for distances up to 8 mm. Above some critical gap distance, however, the electric field strength is no longer high enough to obtain a reliable spark discharge. The  $\epsilon_{eff}$  curves tend to vary linearly with capacitance,  $C$ , at low  $C$  values, but eventually level off at higher  $C$  values. It would appear that some fraction of the stored charge is necessary to generate the electron avalanche in the discharge volume and to initiate

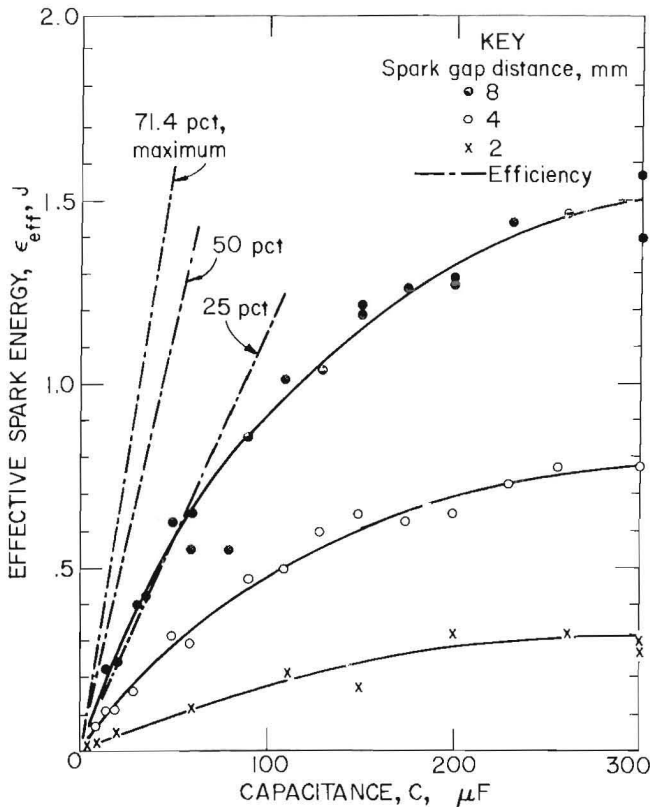


FIGURE 12. - Effective spark energies as a function of capacitance for a test volume of 0.147 L at a charging potential of 300 V.

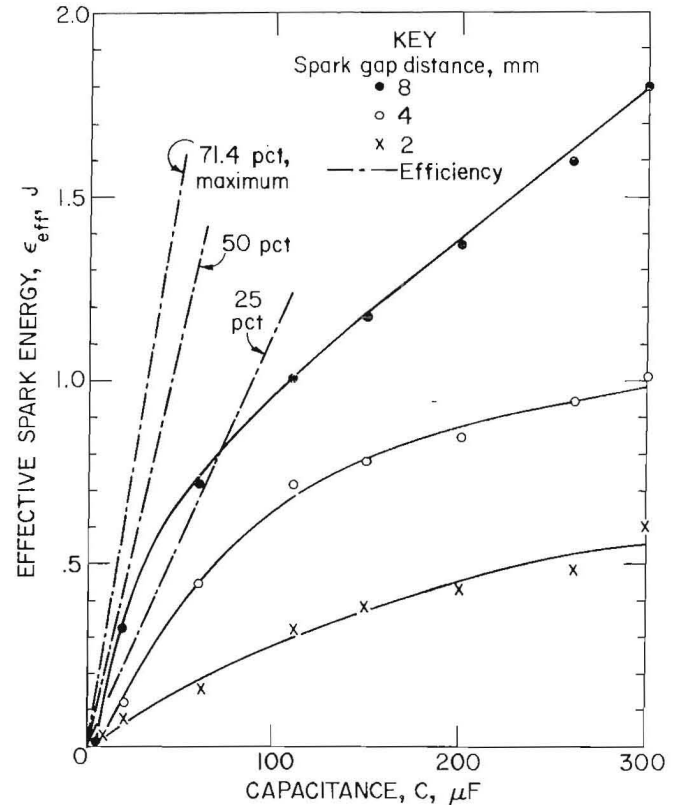


FIGURE 13. - Effective spark energies as a function of capacitance for a test volume of 0.379 L at a charging potential of 300 V.

and establish the arc and glow discharge. That fraction appears efficiently in  $\epsilon_{\text{eff}}$ ; however, once the conducting channel is well established between the electrodes, the gap impedance becomes low and the additional charge that may remain on the capacitor then tends to be dissipated more in the external circuitry than in the discharge gap. The larger the distance between the electrodes, the larger the fraction of the charge that can appear as  $\epsilon_{\text{eff}}$ . A limit is reached when the gap distances are so large that the electric field strength becomes too low to initiate the breakdown avalanche or to maintain it effectively. The efficiency of transfer of the stored electrical energy,  $1/2 CE^2$ , into effective ignition energy,  $\epsilon_{\text{eff}}$ , may be defined as

efficiency (pct) =

$$(100) (2.5 V_0 \Delta p) / (1/2 CE^2). \quad (15)$$

Lines of constant efficiency are also drawn in figures 12 and 13. It is clearly impossible for 100 pct of  $E_1$  to appear as  $\epsilon_{\text{eff}}$ , since a fraction of the deposited energy must appear as the work of compression for the unaffected volume surrounding the spark volume. From equation 11, for a diatomic gas with  $\nu = 5$ , one obtains  $E_1 = 3.5 V_0 \Delta p$ . Since only  $2.5 V_0 \Delta p$  can appear as  $\epsilon_{\text{eff}}$ , the maximum possible efficiency of conversion of stored electrical energy to effective ignition energy is  $100 (2.5/3.5) = 71.4$  pct even if there are no losses in the electrical circuit. The measured efficiencies fall well below that maximum value. The largest measured efficiency values in figure 13 occur for the largest gap distance of 8 mm at low capacitance values. That measured efficiency of about 35 pct for those conditions indicates that about half of the maximum possible effective energy has appeared in the discharge

volume. The remaining energy was probably dissipated as heat in the external circuitry (transformer, leaks, etc.), as heat at the electrodes, as shock energy, or as radiant energy absorbed by the walls. Comparison of the data in figure 12 for a test volume of  $V_0 = 0.147$  L with the data in figure 13 for a larger test volume of  $V_0 = 0.379$  L shows some sensitivity to test volume at the smaller gap distances. Such a dependence on test volume is unexpected on the basis of the analysis presented earlier in equations 2 to 14.

Additional data were obtained in larger test volumes, and the data from the four test volumes for a fixed gap distance of 6 mm are summarized in figure 14. The smaller energy sparks had to be tested in the smaller volumes in order to obtain a measurable pressure rise. The highest energy sparks gave measurable pressure rises in volumes up to 20.2 L. In general, the measured  $\epsilon_{\text{eff}}$  was larger in the larger volumes for any given electrical energy. This sensitivity to test volume decreased as larger volumes were used. In the spark ignitability data to be presented in the following section, the spark energies will be specified in terms of the values for  $\epsilon_{\text{eff}} = 2.5 V_0 \Delta p$  measured in the largest volume in which the pressure for that spark was measured.

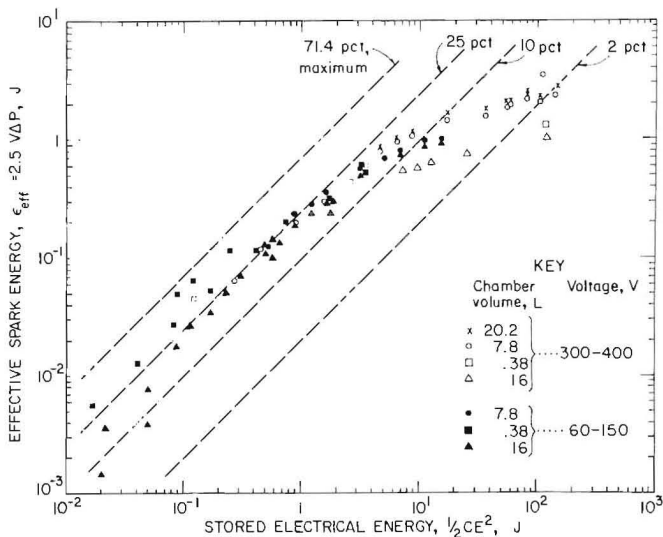


FIGURE 14. - Effective spark energies as a function of stored electrical energy for several test volumes and charging potentials.

The maximum measured efficiency of conversion from stored electrical energy to effective spark energy ranges from 25 to 60 pct. That maximum efficiency is approached at the lower energies, which correspond to the lower capacitances. At the higher energies or capacitance, the efficiency of conversion drops dramatically for reasons to be discussed. Even though more charge may be available at the higher capacitance values, that additional charge is transferred through the system only after the electron avalanche discharge has been created and the arc and glow discharges have been established. By that time the gap resistance may be so low that additional stored energy is deposited less effectively into the discharge gap.

A few of the data points in figure 14 at an electrical energy of 0.1 to 0.3 J show higher efficiencies. These data are for oil-filled capacitors, which are more efficient at transferring charge through the transformer to the spark gap than the polarized electrolytic capacitors used for most of the data.

All of the data in figure 14 are for  $\epsilon_{\text{eff}} = 2.5 V_0 \Delta p$  measured at room temperature in air. In some separate experiments  $\epsilon_{\text{eff}}$  was measured for sparks at elevated temperatures. For the lower energy sparks with an initial room temperature  $\epsilon_{\text{eff}}$  of 0.004 to 0.3 J, the efficiency at 100° C decreased to about 40 to 50 pct of its initial value. For the higher energy sparks, the decline in efficiency with temperature was much less.

The efficiency of some high-energy sparks was also tested in the presence of dust dispersed in the 20-L chamber. Using  $\text{KHCO}_3$  (a dust which decomposes but is nonflammable), the spark efficiency at 500 g/m<sup>3</sup> decreased to about 65 pct of its initial value; at 1,000 g/m<sup>3</sup>, it decreased to 40 pct. Other dusts which may decompose or pyrolyze by varying amounts may affect the spark differently.

This decrease in spark efficiency at elevated temperatures and in the presence of dust must be considered when reading the remainder of this report. However, because of the great difficulty in determining the true spark efficiency at each temperature and dust concentration, the

spark effective energies,  $\epsilon_{\text{eff}}$ , listed in this report are only the values measured at room temperature in air in the absence of dust.

## ELECTRICAL IGNITABILITY DATA

### Pittsburgh Seam Coal

An example of the detailed spark ignition data for Pittsburgh seam coal dust in the 1.2-L furnace is shown in figure 15. The thermal ignitability and lean flammability limit curves are taken from figure 9. The data are the ignition and nonignition points at an effective spark energy of 0.250 J (or a stored electrical energy of 1.08 J). The points are delineated within the intermediate domain of temperatures and dust concentrations that are flammable but not thermally autoignitable. With the addition of a relatively moderate spark source of 0.250 J, a large area becomes an ignitable domain with an explosion probability of unity. The spark ignitability curve drawn to separate the ignitable domain from the nonignitable domain dips down to a minimum that just barely includes room temperature. That minimum energy for room temperature ignition occurs at a narrow range of dust concentrations between 775 and 800  $\text{g}/\text{m}^3$ .

The coal dust data for all the spark energies studied in the 1.2-L furnace are summarized in figure 16. Curve *c* for  $\epsilon_{\text{eff}} = 0.250$  J is based on figure 13. The other spark ignitability curves were drawn from similar data at the other spark energies. The thermal ignitability and lean flammability limit curves that define the intermediate domain were again taken from figure 9.

At the highest effective spark energy studied,  $\epsilon_{\text{eff}} = 1.360$  J (curve *a*), most of the intermediate domain at the higher concentrations is spark ignitable. No rich ignitability cutoff was observed at that energy out to concentrations as high as 1,800  $\text{g}/\text{m}^3$ . For coal, the lean ignitability curve at that highest energy, curve *a*, is substantially displaced from the lean flammability limit at all temperatures. Previously reported data have

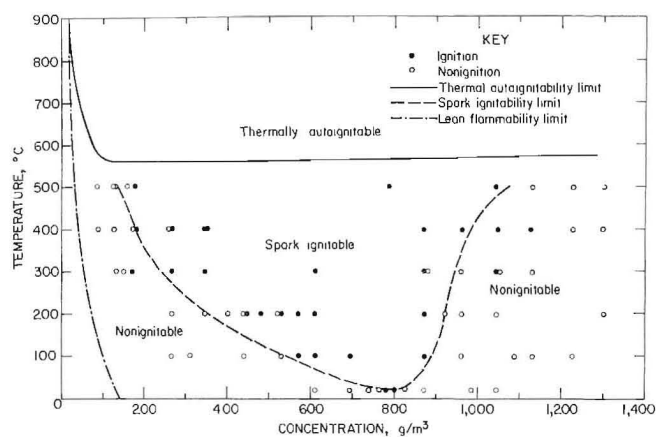


FIGURE 15. - Ignition and nonignition data points at an effective spark energy of 0.250 J for minus 200-mesh Pittsburgh coal in the 1.2-L furnace.

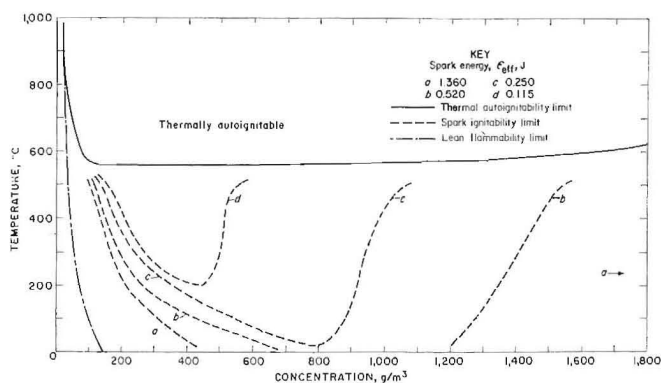


FIGURE 16. - Spark ignitability data for minus 200-mesh Pittsburgh coal in the 1.2-L furnace at various spark energies.

shown that pyrotechnic ignition energies of the order of hundreds of joules were required in order for the coal dust ignitability curve to become coincident with the true lean limit of flammability at room temperature (25, 27).

The ignitability curve *b* for the next lowest energy,  $\epsilon_{\text{eff}} = 0.520$  J, is shifted still farther away from the true lean flammability limit curve in figure 16. This lower energy curve displays a rich ignitability cutoff in the concentration range of 1,300 to 1,500  $\text{g}/\text{m}^3$ . The data at still lower energies, curves *c* and *d*, show a continuous narrowing of the ignitability domain with decreasing spark energy. The 0.250-J curve barely dips

below room temperature at dust concentrations in the range of 775 to 800 g/m<sup>3</sup>. The 0.115-J curve *d* shows no ignitability at room temperature in the 1.2-L furnace apparatus.

The lean ignitability curves show a continuous displacement from the true lean flammability limit curve as the spark energies decline. However, the narrowing of the ignitability domain occurs predominantly by a reduction of the rich cutoff concentration with decreasing spark energy. The sharp cutoff, together with the scatter in the data on the rich side, suggests that the cause may be a direct physical interaction between the coal dust cloud and the spark channel discharge. The dust cloud is an array of dense, solid objects that are electrically isolated from the spark electrodes. They are in the air space that will eventually become the electrical discharge channel when the spark is energized. When the electron avalanche is generated, the insulated dust particles will take on an electric potential that is determined by the mobility difference between the positive and negative charge carriers in the discharge channel. The dust particles' electric potential is thus not externally controllable. At low dust concentrations, the electric discharge channel in the air space around the dust particles is perturbed only slightly by the presence of those particles. The ions and electrons of the avalanche can readily flow around them. At elevated dust concentrations, however, the particles will absorb or divert an increasingly larger fraction of the discharge energy. Energy that would normally go into the electron-ion avalanche process is absorbed and dissipated by the presence of such a flowing, concentrated array of insulated, energy-absorbing particles. As discussed in the section on "Effective Spark Energies," the efficiency of the sparks was measured in the presence of a dust cloud and found to decrease with increasing dust concentrations, but the  $\epsilon_{\text{eff}}$  values listed in the figures were measured in air in the absence of dust.

The spark ignitability of Pittsburgh coal dust was also measured in the 8-L

and 20-L chambers, and the data are shown in figure 17. In this case, the dust was 85 pct minus 200 mesh and had  $\bar{D}_s = 27 \mu\text{m}$  and  $\bar{D}_w = 46 \mu\text{m}$ , slightly larger than the dust used in the 1.2-L furnace and listed in table 1. Its proximate and ultimate analyses are similar to those in table 1. The 8-L and 20-L data are very similar. The spark ignitability solid curve for the 20-L data is drawn through the 0.5-s delay points, which were somewhat lower than the 0.1-s delay data. Perhaps the reduced turbulence for the

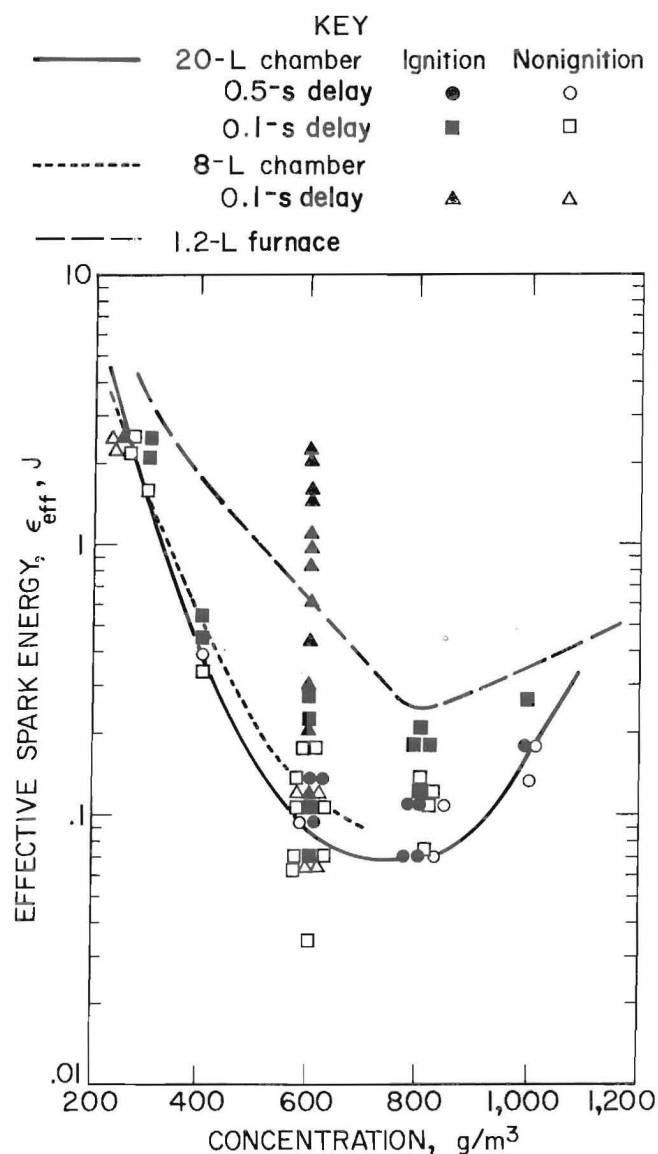


FIGURE 17. Spark ignitability data for Pittsburgh coal in the 8-L and 20-L chambers compared with 12-L furnace data at room temperature.

longer delay made the dust easier to ignite. The 8-L and 20-L data are also compared to the room temperature data in the 1.2-L furnace derived from the data in figure 16. The general shapes of the curves are similar with minima at about  $800 \text{ g/m}^3$ , but the 1.2-L furnace data are higher at all concentrations. The differences are probably related to differences in dispersion turbulence and dust cloud uniformity between the furnace and the two chambers. The minimum spark ignition energy for Pittsburgh coal dust in the 20-L chamber is about  $0.070 \text{ J}$  for  $\epsilon_{\text{eff}}$ , or about  $0.31 \text{ J}$  stored electrical energy.

### Lycopodium

An example of the detailed spark ignitability data in the 1.2-L furnace for lycopodium is shown in figure 18. The thermal ignitability and lean flammability limit curves that define the intermediate domain are taken from figure 10. The data are the ignition and nonignition points at an effective spark energy of  $0.050 \text{ J}$  (or a stored electrical energy of  $0.090 \text{ J}$ ). Those ignition and nonignition points are within the intermediate domain of temperatures and dust concentrations that are flammable but not thermally autoignitable. As can be seen, in the

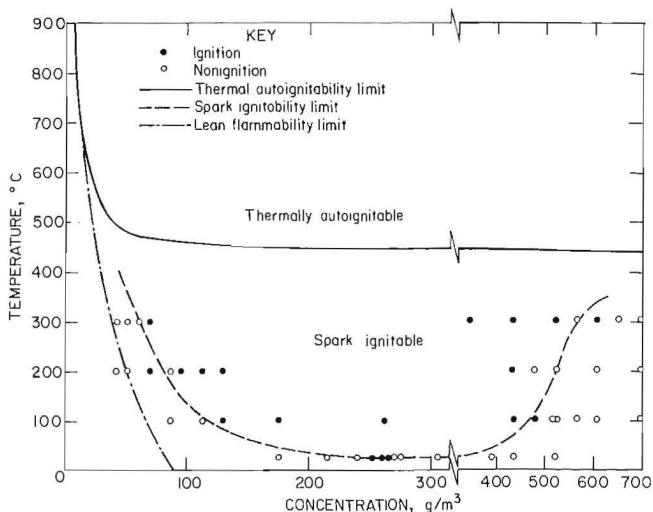


FIGURE 18. - Ignition and nonignition data points at an effective spark energy of  $0.050 \text{ J}$  for lycopodium in the 1.2-L furnace.

presence of a relatively weak spark source of  $0.050 \text{ J}$ , a large area of that domain becomes an ignitable domain with an explosion probability of unity. A spark ignitability curve (dashed) has been drawn to separate the domain that is spark ignitable from the regions that are nonignitable at that spark energy. The curve dips down with a broad minimum that just barely reaches room temperature. Thus a lycopodium dust concentration of  $260 \text{ g/m}^3$  in air at  $25^\circ \text{ C}$  is just barely ignitable with a spark energy of  $\epsilon_{\text{eff}} = 0.050 \text{ J}$ . Higher and lower concentrations at that initial temperature are not ignitable with that spark source. There is more scatter in the data on the rich side of the spark ignitability curve than on the lean side of the curve. That larger scatter was generally observed for most of the spark energies studied. It is probably related to the mechanism by which the spark ignition process is partially quenched by high dust loadings, as discussed previously.

The lycopodium data for all the spark energies studied are summarized in figure 19. Curve *e* for  $\epsilon_{\text{eff}} = 0.050 \text{ J}$  is taken from figure 18. The other spark ignitability curves in figure 19 were drawn from similar data points at their respective spark energies. For curve *a*, the highest spark energy at  $\epsilon_{\text{eff}} = 1.360 \text{ J}$ , virtually the entire intermediate domain that is accessible to the experimental

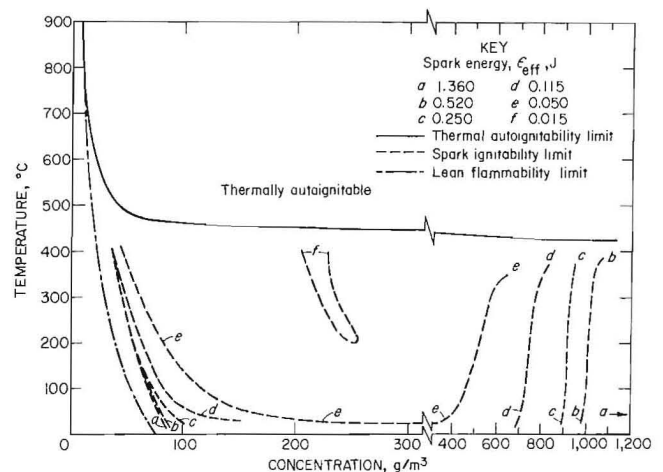


FIGURE 19. - Spark ignitability data for lycopodium in the 1.2-L furnace at various spark energies.

system is spark ignitable. The lean ignitability curve at that highest spark energy studied is close to the lean flammability limit contour based on the Burgess-Wheeler law. No rich ignitability curve was observed at that spark energy even with dust loadings as high as  $1,300 \text{ g/m}^3$ . The data show that in the presence of a spark energy of  $1.360 \text{ J}$ , explosion is certain for virtually all flammable mixtures studied. That ignitability curve (*a*) stops at room temperature simply because lower temperatures are not accessible to the 1.2-L system as it is presently designed. There is little doubt, however, that explosion is virtually certain for flammable mixtures at temperatures well below room temperature.

The ignitability curve *b* for the next lowest energy,  $\epsilon_{\text{eff}} = 0.520 \text{ J}$ , is virtually identical with the higher energy curve *a* on the lean side. The rich ignitability portion of curve *b*, however, displays a relatively sharp cutoff at a dust concentration of  $1,000 \text{ g/m}^3$ . It should be noted that the thermal autoignition curve immediately above curve *e*, at a temperature of  $420^\circ \text{ C}$ , is still perfectly flat at that concentration and shows no evidence of any rich-limit behavior. That thermal autoignitability curve shows no tendency to turn upward even at concentrations above  $1,300 \text{ g/m}^3$ . If one were dealing with a true rich-limit behavior at a dust concentration near  $1,000 \text{ g/m}^3$ , then both the thermal and the spark ignitability curves would show an upward trend in the same concentration regions. Yet only the spark ignitability curve shows that upward trend, and it does so without the gradual curvature that one would expect for the temperature dependence of a true rich limit. Instead, the spark ignitability cutoff is almost discontinuous at a discrete dust concentration of  $1,000 \text{ g/m}^3$ , which is almost independent of the initial temperature. That contrasting behavior, together with the scatter in the data at those rich cutoffs, suggests that the cause of those cutoffs may be related to the specific, direct physical interaction between the dust cloud and the spark channel.

The data at still lower energies (curves *c*, *d*, *e*, and *f*) show a continuous narrowing of the ignitability domain with decreasing spark energy. The  $0.050\text{-J}$  curve barely reaches room temperature at a dust concentration of about  $260 \text{ g/m}^3$ . The  $0.025\text{-J}$  ignitability curve shows no ignitability at room temperature. It should be noted that the narrowing of the ignitability domain occurs predominantly by a reduction of the rich cutoff concentration with decreasing spark energy. On the lean side, there is very little change until the lowest energies are reached. At the higher energies the lean curves tend to bunch close to the lean limit of flammability. Note that as the spark energies are decreased, the curves first begin to separate from the lean flammability limit contour at the lower temperatures. For curve *f*, the separation from the lean flammability curve is marked at all temperatures and only a narrow concentration range is ignitable. It is interesting to note that the narrow peninsula of ignitability that remains at  $\epsilon_{\text{eff}} = 0.025 \text{ J}$  slopes in a direction that is consistent with the expectation that the maximum in ignitability should correspond to a near-stoichiometric ratio of fuel to oxygen. The mass concentration of  $\text{O}_2$  in the furnace at  $400^\circ \text{ C}$  is significantly lower than the mass concentration of  $\text{O}_2$  at  $200^\circ \text{ C}$ . The direction of the slope in the narrow peninsula of ignitability is in that same direction. Note that the lean flammability limit curve has a parallel slope for essentially the same reason.

#### Modified Burgess-Wheeler Law and Lycopodium

As mentioned earlier, the Burgess-Wheeler law (equation 1) will now be derived. Nearly a century ago LeChatelier and Boudouard (32) had noted that the limit calorific values for a variety of hydrocarbon fuels were approximately constant at about  $12 \text{ kcal/mol}$  of fuel-air mixture at the lean flammability limits. Somewhat later, Burgess and Wheeler (7) investigated the matter in more detail and found that for the first five members of the paraffin series of hydrocarbons,

the heat liberated by the combustion of 1 mol of a lean limit mixture in air, at room temperature, was nearly constant. If  $L_{25}$  is the measured lean limit in mol (or volume) percent at 25° C and if  $\Delta H_c$  is the fuel's heat of combustion, it was that product,  $L_{25} \Delta H_c$ , the limit calorific value, that Burgess and Wheeler had found to be constant for the n-saturated hydrocarbons.

More recently, Burgess and Hertzberg (6) and Hertzberg (20) showed that kinetic factors and their interplay with natural convection exert a dominant role in determining the lean-limit concentrations. They showed that the limit calorific values varied appreciably from one homologous series of organic fuels to another as their reactivity factors varied appreciably. However, within the series of paraffin hydrocarbons the oxidation rates are limited by rate-determining steps that involve the same single carbon atom fragments, and hence the overall reactivity factors are nearly identical within the homologous series of paraffins (46). Accordingly, the limit calorific values for the paraffins are nearly invariant, as observed by Burgess and Wheeler (7).

The quantity  $L_{25} \Delta H_c$  is the minimum combustion enthalpy that must be supplied by the oxidation reaction in order to sustain flame propagation. That minimum enthalpy generates a certain limit flame temperature (in degrees Celsius) in the burned gases that is given by

$$(T_b)_l = 25 + L_{25} \Delta H_c / c \quad (16)$$

where  $c$  is the effective heat capacity of the system. Since  $L_{25} \Delta H_c$  was approximately constant for the paraffin hydrocarbons and since  $c$  is the heat capacity of a mixture consisting mostly of air at the lean flammability limit, it is not surprising that the paraffin hydrocarbons all have approximately the same lean-limit flame temperature of about 1,300° C (49).

Now at some elevated temperature,  $T$ , an additional sensible enthalpy,  $c(T-25)$ , is available to the reactants. The total enthalpy available to the system when it reacts at the higher initial temperature

is the sum of chemical and sensible enthalpies. That total enthalpy at the higher temperature is  $L_T \Delta H_c + c(T-25)$ . If the minimum enthalpy required at the standard temperature of 25° C is  $L_{25} \Delta H_c$ , then that minimum is attained at the higher initial temperature when

$$L_{25} \Delta H_c = L_T \Delta H_c + c(T - 25). \quad (17)$$

Solving equation 13 for the lean flammability limit at the higher temperature gives

$$L_T = L_{25} \left[ 1 - \frac{(T - 25)}{L_{25} \Delta H_c / c} \right]. \quad (18)$$

In terms of the lean-limit flame temperature defined in equation 16, equation 18 becomes

$$\begin{aligned} L_T &= L_{25} \left[ 1 - \frac{T - 25}{(T_b)_l - 25} \right] \\ &= L_{25} [1 - \gamma (T - 25)], \end{aligned} \quad (19)$$

where  $\gamma$  is a constant equal to  $0.00078^\circ \text{C}^{-1}$  for the n-saturated hydrocarbons where  $(T_b)_l \approx 1,300^\circ \text{C}$ . The measured value of  $0.00072^\circ \text{C}^{-1}$  from the empirical B-W law (equation 1) is in fair agreement with that prediction. Since equations 18 and 19 were derived on the assumption of a constant limit calorific value, they are referred to as the modified Burgess-Wheeler Law (47). In reality, the limit calorific value can vary from one homologous series of organic fuels to another, and the temperature coefficient should vary as well. The more reactive fuels with low limit calorific values and lower limit flame temperatures should have lean limits that are more sensitive to temperature than the less reactive fuels. In general terms, for any fuel, the Burgess-Wheeler law may be generalized in the form of the simple linear relationship

$$L_T = L_{25} [1 - \beta(T - 25)], \quad (20)$$

where  $\beta$  is a temperature coefficient whose value depends on the limit flame temperature of the fuel.

As given above,  $L_T$  and  $L_{25}$  are lean flammability limits at temperature  $T$  and at room temperature  $25^\circ\text{C}$ , respectively, and are expressed as mol percent or volume percent of fuel in the fuel-air mixture. To apply the equation to dusts, the fuel concentrations must be expressed in terms of the mass concentration of fuel per unit volume.

For a gaseous fuel with a lean-limit composition of  $L_T$  mol percent, the corresponding lean-limit mass concentration of fuel per unit volume is

$$C_T = \frac{L_T}{100} \rho_T, \quad (21)$$

where  $\rho_T$  is the mass density of the pure fuel at temperature  $T$ . Substituting equation 21 and the similar expression for  $C_{25}$  into equation 20 gives

$$C_T = C_{25} \frac{(\rho_T)}{(\rho_{25})} [1 - \beta(T - 25)]. \quad (22)$$

However, according to the ideal gas law

$$\rho_T = \frac{pM}{R(T + 273)}, \quad (23)$$

where  $R$  is the gas constant,  $T$  is the temperature in degrees Celsius,  $p$  is the pressure, and  $M$  is the fuel molecular weight. Therefore, at a constant pressure for any given fuel,  $\rho_T/\rho_{25} = (273 + 25)/(T + 273)$ . Thus in terms of the mass concentration of fuel at the lean flammability limit, the Burgess-Wheeler law becomes

$$C_T = C_{25} \left( \frac{298}{T + 273} \right) [1 - \beta(T - 25)]. \quad (24)$$

Thus equation 24 expresses the expected temperature coefficient for the lean limit of flammability of a condensed-phase fuel such as a dust where the limit composition must be measured in terms of the mass concentration of fuel per unit volume. This equation was used to delineate the flammability domains for coal, lycopodium, and polyethylene dusts shown in figures 9, 10, and 11.

The ignitability data for lycopodium presented in figure 19 provided a surprising bonus. The dust was so easy to ignite that it was possible to approach the true lean limit of flammability with the spark energies used. That is rather rare for dusts, and the data obtained provide an independent test of the validity of the modified Burgess-Wheeler law for lycopodium. The 1.2-L furnace data from figure 19 are presented in figure 20 in a different format. The ignition and nonignition points for lycopodium are plotted on a logarithmic graph of spark energy versus dust concentration at constant furnace temperatures. Figure 20A is for the room temperature data at  $20^\circ$  to  $27^\circ\text{C}$ , figure 20B for  $100^\circ\text{C}$ , figure 20C for  $200^\circ\text{C}$ , figure 20D for  $300^\circ\text{C}$ , figure 20E for  $400^\circ\text{C}$ , and figure 20F for  $500^\circ\text{C}$ . At that highest temperature, the system is thermally autoignitable for all concentrations above  $39\text{ g/m}^3$  (see fig. 10). The dashed curves drawn in figure 20 separate the regions that are spark ignitable from those that are nonignitable at the temperature studied. The slopes of the curves are similar to those obtained for other types of fuels including gases and dusts (25). The real limits of flammability are those that are independent of ignition energy (20); namely, the vertical asymptotes in the figures. At lower energies, where the curves have finite slopes, it is only the ignitability of the mixture that is being measured. While there is considerable scatter in the data, they clearly show a systematic decrease in that "true" or asymptotic lean flammability limit with increasing initial temperature.

Those asymptotic lean flammability limits from the spark data in the 1.2-L furnace are plotted as a function of the initial temperatures in figure 21. The dashed curve through the high-spark-energy lean-limit data points represents the resultant measured lean limit as a function of the initial temperature. The solid curve is the measured thermal autoignitability limit from figure 10. The dot dashed curve is the B-W law extrapolated from the measured room temperature

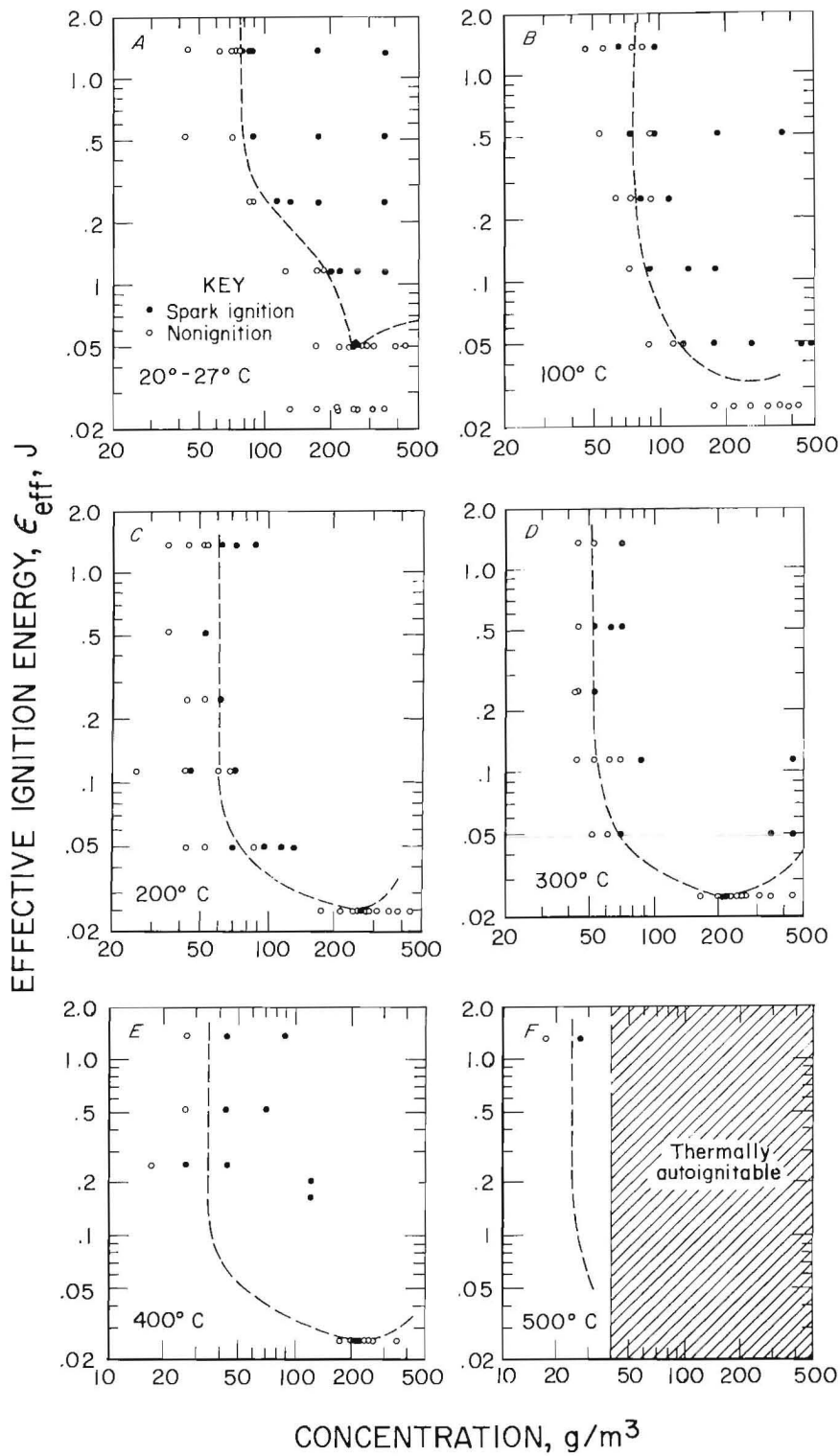


FIGURE 20. - Spark ignition energy versus dust concentration for lycopodium in the 1.2-L furnace at room temperature and elevated temperatures. Dashed curves separate regions that are spark ignitable from those that are not ignitable at temperature studied.

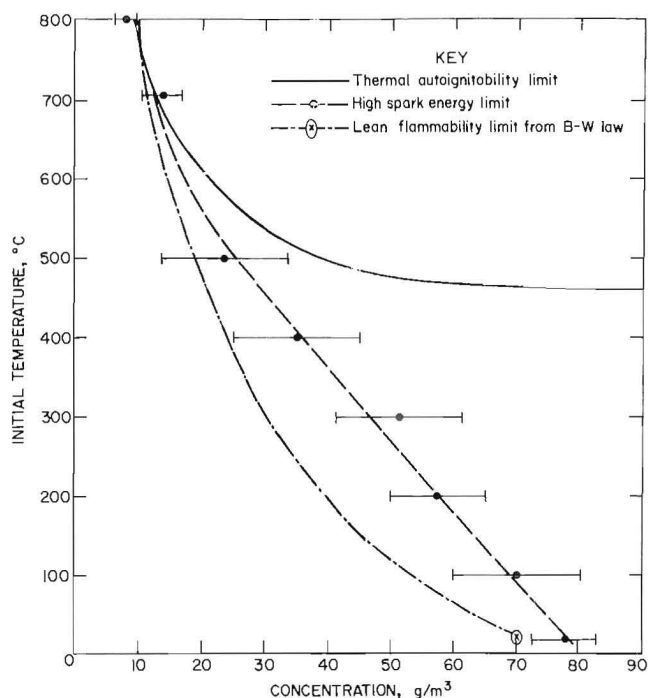


FIGURE 21. - Temperature dependence of the lean flammability limit for lycopodium in air. Data obtained at high spark energies compared with the modified Burgess-Wheeler law.

lean flammability limit in the 20-L chamber. Above some elevated temperature, it is reasonable to expect that thermal autoignition would occur spontaneously at the lean flammability limit concentration. The fact that the high-spark-energy lean-limit curve connects with that ignitability curve at those elevated temperatures tends to confirm that expectation. Accordingly, the two data points on the thermal ignitability curve at 700° and 800° C are also taken to be the measured lean limits at those temperatures. The lean flammability limit curve through the high-spark-energy points at the lower temperatures is therefore extended upward through those higher temperature data points.

The measured lean flammability limit for lycopodium in the 20-L chamber is 70 g/m<sup>3</sup> with a precision of ±10 g/m<sup>3</sup>. For lycopodium, the volatile constituents that are involved in the gas-phase oxidation reactions that control its flammability contain substantial amounts of

oxygen linkages in their structure. Because they are, therefore, already partially oxygenated, their expected lean-limit flame temperature is probably higher than the value for the n-saturated hydrocarbons. Accordingly, the temperature coefficient  $\beta$  is taken as the somewhat lower value of  $\beta = 0.00064^\circ \text{C}^{-1}$ .

Therefore, the B-W curve (equation 24) or predicted lean flammability limit at elevated temperatures for lycopodium is

$$C_T = \left[ 70 \frac{298}{T + 273} \right] [1 - 0.00064 (T - 25)] \text{ g/m}^3. \quad (25)$$

The precision of the measured spark lean limits from figure 20 is shown on figure 21. The uncertainty in the absolute concentrations in the 1.2-L furnace and the 20-L chamber is undoubtedly larger than the precision of the measurements. Therefore, within the total experimental error of the measurements, the high-spark-energy data for the lean flammability limits of lycopodium at elevated temperatures confirm the applicability of the B-W law to lycopodium dust.

The spark ignitability of lycopodium at room temperature was also measured in the 20-L chamber, and the data are shown in figure 22. Ignition and nonignition points and the solid curve through them show the spark ignition energy as a function of dust concentration in the 20-L chamber. These data are compared to the dashed line derived from the 1.2-L furnace data in figure 19. The general shapes of the curves are similar. As with the Pittsburgh coal data, the small differences may be related to differences in dust cloud uniformity or turbulence level between the 1.2-L furnace and 20-L chamber. The minimum spark ignition energy in the 20-L chamber is  $\epsilon_{\text{eff}} = 0.035$  J, or a stored electrical energy of 0.170 J.

#### Polyethylene

The detailed 1.2-L furnace spark ignition data for polyethylene shown in figure 23 reveal some unexpected

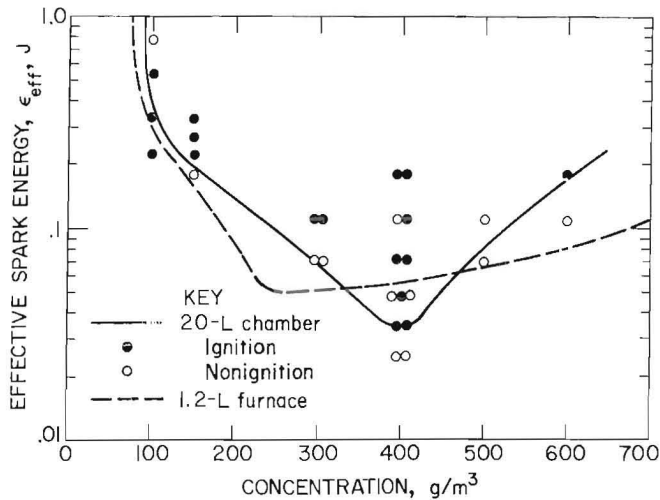


FIGURE 22. - Spark ignitability data for lycopodium in the 20-L chamber compared with 1.2-L furnace data at room temperature.

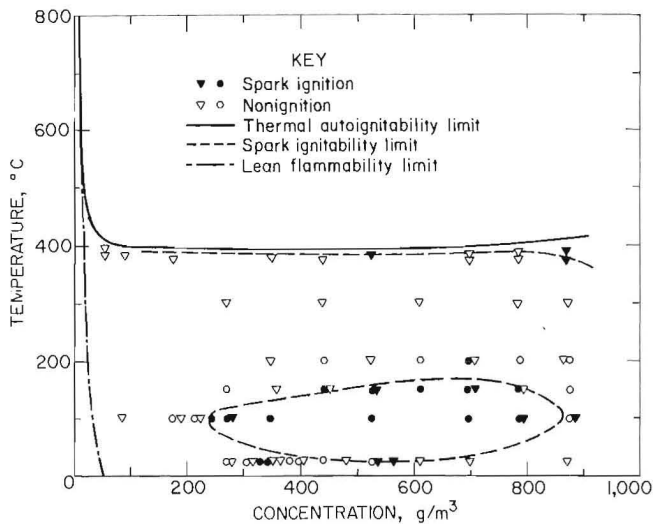


FIGURE 23. - Ignition and nonignition data points at an effective spark energy of 0.070 J for polyethylene in the 1.2-L furnace. Triangular data points are for a series of tests with increasing furnace temperature, and circular data points are for test series with decreasing furnace temperatures.

complications. The data points corresponding to ignitions and nonignitions at an effective spark energy of 0.070 J or a stored electrical energy of 0.120 J are plotted in temperature versus dust concentration space. The ignition and nonignition points are plotted in the intermediate domain for various combinations of initial temperature and dust concentration that are flammable but not

thermally autoignitable. A spark ignitability curve has been drawn to separate the ignitable regions from the domain that is nonignitable at that spark energy. The triangular data points are from a series of tests using the normal procedure of increasing the furnace temperature to reach the next test temperature. The circular data points are from a test series made by decreasing the furnace temperature to reach the next test temperature. This second series showed that there was no hysteresis effect from the past history of the chamber.

The complication for polyethylene is obvious from the shape of that curve. In the intermediate temperature regions the curve completely closes on itself! In all cases previously studied, the regions were unbounded from above and the ignitability domains at the higher temperatures were always wider than at the lower temperatures. The ignitability curve in figure 23 is thus in marked contrast to the curve for lycopodium (fig. 18) and the curve for coal dust (fig. 15). In the latter two cases, for the energies shown, the ignitability curves displayed a relatively broad minimum that dipped down to touch room temperature, but in both previous cases the regions had no upper bound. By contrast, while the polyethylene curve displays the same type of broad minimum, it is bounded from above by a strange maximum. Thus for polyethylene, there are higher temperature regions above 100° C that are less ignitable than regions at 100° C. In fact above the maximum at 175° C, there is a domain of temperatures that is entirely nonignitable for that spark energy regardless of the dust concentration. Yet at most concentrations and at lower temperatures, the dust is readily ignited. This behavior for polyethylene was entirely unexpected and markedly different from the "normal" behavior that was observed for the other two dusts.

Some hints as to the cause of polyethylene's behavior are provided by figure 24, which summarizes the data at other spark energies studied. The family of curves shows clearly that the same anomalous behavior is observed regardless of

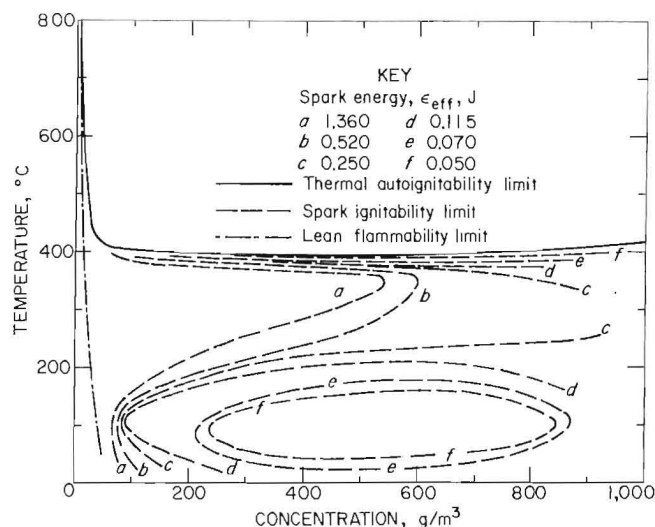


FIGURE 24. Spark ignitability data for polyethylene at various spark energies in the 1.2-L furnace.

the spark energy. All the ignitability curves show reversal of curvature at a temperature just above  $100^{\circ}\text{C}$ . The higher energies (curves *a* and *b*) show the same curvature reversal even though they do not form closed "islands." At still higher temperatures, as the thermal autoignition curve is approached, the curvatures reverse again and display the normal behavior.

It is no coincidence that the anomalous curvature begins at the same temperature regardless of the spark energy. It is also no coincidence that that temperature is near  $115^{\circ}\text{C}$ , which is the point at which polyethylene begins to melt. That softening temperature was confirmed by differential thermal analyses (DTA) of the dust at heating rates of 10 and  $50^{\circ}\text{C}/\text{min}$ . The DTA confirmed a softening or melting endotherm that began at  $115^{\circ}\text{C}$ . By  $135^{\circ}\text{C}$  the powdered polyethylene sample in the DTA was completely molten and fused into one large mass. Subsequent decomposition or devolatilization of the polyethylene sample did not begin until much higher temperatures were reached. Clearly, any solid dust particles that are dispersed at  $115^{\circ}$  to  $135^{\circ}\text{C}$  would melt as they reached the furnace temperature. When impacting the walls or the spark electrodes, the softened or liquid droplets of fuel would tend to stick and to concentrate on those

surfaces. The adhering dust particles are thus effectively removed from the spark channel volume and the surrounding test volume, and their effective concentration is reduced. It is thus more difficult to achieve ignition in the presence of such melting, and a higher initial concentration is required to achieve ignition. Even if the molten particles only impact each other, they will still tend to adhere so that the effective particle diameter increases. That increase in effective diameter also reduces the flammability of the dust and requires a higher initial concentration in order to achieve ignition (26). Thus the ignitability contours shift toward higher concentrations as the temperature increases above the melting range of  $115^{\circ}$  to  $135^{\circ}\text{C}$ , resulting in a reversal of the normal curvature. For the lower spark energies, in particular, the reversal occurs more rapidly, and at some point the reversing curve reaches the normal rich-limit cutoff. At that point a completely closed loop or island is formed, isolating the ignitable domain below the melting temperature from the nonignitable regions above the melting temperature.

If the above explanation of the anomalous behavior is correct, then the detailed shapes of the ignitability curves above  $115^{\circ}\text{C}$  should be sensitive to the detailed experimental procedure. In particular they should be sensitive to the details of the time delay between the dispersion pulse and the activation of the spark discharge. A certain minimum delay is necessary for the cold dust to disperse effectively and to reach oven temperature. However, a very long delay above the melting temperature will provide a longer time for dust particles to be lost by adhesion to surfaces and by impact agglomeration. In these experiments the time delay was fixed so that the spark was energized some 40 ms after the dispersion pulse was completed. That time was quite sufficient for the injected dust cloud to reach oven temperature before the spark was energized. In those cases where the oven temperature exceeds the melting temperature, there is a significant time for the molten particles to

be lost by surface impact and agglomeration. The anomalous behavior for polyethylene persists until much higher temperatures are reached and the thermal autoignitability curve is approached. The normal behavior is not reestablished until those elevated temperatures are reached. It is reestablished when devolatilization and autoignition of the vapor-air mixture occur very rapidly. Those higher temperatures also correspond to higher heating rates. Under those conditions volatilization occurs so rapidly after melting that there is no significant time available for collisional losses by surface adhesion or agglomeration. At the higher temperatures, therefore, melting, volatilization, gas phase mixing, and ignition occur before there is any significant loss. Furthermore, liquid polyethylene vaporizing from electrodes, or from large liquid agglomerates, is still contributing fuel to the initial spark volume between the electrodes. Similarly, vaporizing fuel adhering to the walls is still contributing fuel to the test volume.

The spark ignitability at room temperature was also measured in the 20-L chamber. The ignition and nonignition data points and the solid curve through them in figure 25 show the spark ignition energy as a function of dust concentration. These 20-L data are compared to the 1.2-L furnace data (dashed curve) derived from

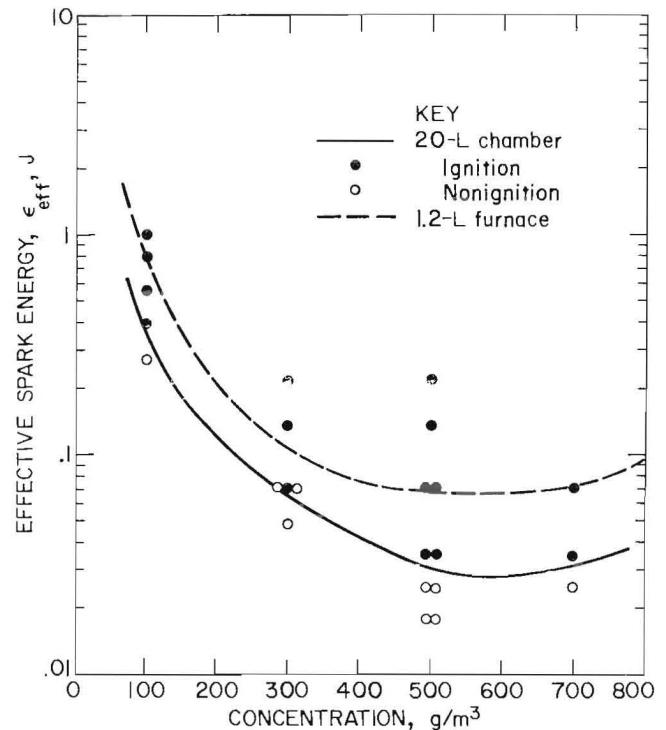


FIGURE 25. - Spark ignitability data for polyethylene in the 20-L chamber compared with 1.2-L furnace data at room temperature.

figure 24. The 20-L data show lower spark ignition energies at all concentrations, but the shapes of the two curves are the same, with a minimum at 500 to 600 g/m³. The 20-L chamber minimum spark energy is  $\epsilon_{eff} = 0.030$  J, or a stored electrical energy of 0.140 J.

#### DISCUSSION AND ANALYSIS

The electrical ignition hazard for fuels is traditionally specified in terms of their minimum ignition energies (5). For gases, the available data are by now virtually classical and are based on Bureau of Mines measurements that were initiated some four decades ago (19). For such static gases, the measuring procedures are relatively simple, and the results obtained are in reasonable agreement with the established concepts of combustion theory (33). For dusts, however, while measuring procedures have been proposed (12), and data obtained (40), there is considerable controversy regarding their reliability and relevance, and no established theory exists

to account for the results (3, 13, 31). This discussion and analysis is presented in two parts: The first deals with the specific problem of extending the concept of minimum ignition energies to dusts. The purpose of considering that question involves the larger issue of the classification of the electrical ignition hazards for dusts. The second part of this section is a theoretical refinement of current theories of spark ignition energies for gases. That refinement is necessary in order to provide a logical starting point for the evolution of a theory that would be applicable to dusts.

## CLASSIFICATION OF ELECTRICAL IGNITION HAZARDS

In principle, the minimum ignition energy for a dust dispersed in air is measurable; however, its accurate determination involves extraordinary complications and a fundamental contradiction in the experimental requirements. The extraordinary complications will be considered in detail shortly. The fundamental contradiction deals with the flow requirement. For gases, in order to minimize ignition energies, there should be no flow of the test medium with respect to the electrodes (2, 43, 44). But in order to disperse a dust cloud effectively at a definable concentration, an intense flow disturbance is required (8, 27). This fundamental contradiction prevents the "true" minimum from being reached. It means that the extent to which the true minimum in ignition energy can be approached depends on the details of the dust dispersion method (15), the geometry of the spark gap, its exact location in the dispersing flow, the timing between dispersion and ignition, and other experimental details that may be entirely unrelated to the intrinsic combustion properties of the dust. Thus the extent to which the measurements can approach the true minimum may depend on the ability of the experimentalist to devise some method of dispersing the dust effectively in the spark gap with a minimum level of flow disturbance.

The available data for lycopodium illustrate the dispersion contradiction and the many other extraordinary complications involved in determining minimum ignition energies for dusts. The minimum for lycopodium in the 1.2-L furnace can be inferred from the one ignitability curve (figs. 18-19) that is just tangent to the room temperature ordinate of 25° C. It corresponds to an  $\epsilon_{eff}$  of 50 mJ, and the tangency point occurs at a dust concentration of 260 g/m<sup>3</sup>. The stored electrical energy for that  $\epsilon_{eff}$  value is 90 mJ, and hence, according to the common definition, that is the minimum ignition energy. Earlier Bureau researchers (29) report a minimum electrical energy of 40 mJ at an unspecified dust loading in a

1.2-L Hartman chamber. In a more recent Bureau report, Kubala, Perzak, and Litchfield (31) report a minimum of 30 mJ. They used a 2.7-L volume into which was dispersed a measured dust loading. Although they did not monitor the effectiveness of dust dispersion, it is tentatively assumed that their apparent or nominal dust concentration can be inferred from their mass loading of dust divided by the chamber volume. Their data are compared directly with those reported here in the 1.2-L furnace and 20-L chamber in figure 26. The general shapes of the three curves are similar. However, the minimum spark energy is reached at a concentration of about 260 g/m<sup>3</sup> in the 1.2-L furnace and at higher concentrations of 400 g/m<sup>3</sup> in the 20-L chamber and 400 to 500 g/m<sup>3</sup> in the 2.7-L chamber. The lower minimum spark energy value by Kubala (31) may be due to a lower turbulence level in the chamber or to a more efficient transfer of stored electrical energy to the spark gap. In reality, it will be seen that even the 30 mJ reported by Kubala (31) is higher than the true minimum that would be measured in a

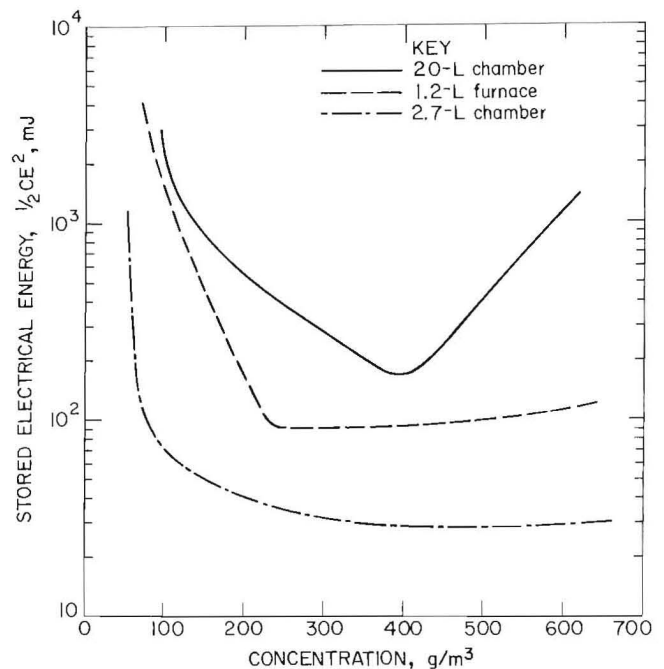


FIGURE 26. - Concentration dependence for the electrical ignitability of lycopodium at room temperature, including comparison of data obtained in this study with earlier Bureau data (31).

static system if it were possible to disperse 300 to 500 g/m<sup>3</sup> of lycopodium dust in such a static air medium.

Eckhoff (13) describes an optimum circuit design that was used to maximize the conversion efficiency of stored electrical energy into "actual spark energy." He also used an optimum discharge duration that was comparable to the optimum duration observed for the spark ignition of gases (30, 43). For the "optimum amount of powder," Eckhoff's minimum energy for a 50-pct probability of ignition was 10 mJ for lycopodium in air. The most recent study by Glarner (17) reports a minimum value of 2 mJ at a nominal dust loading of 100 g/m<sup>3</sup> and a low level of turbulence. The turbulence level in the 20-L chamber used by Glarner was decreased by increasing the delay time between dust dispersion and spark ignition.

In few of these measurements was care taken to ensure that the dust was uniformly dispersed, so the real concentration in the spark gap was unknown. Even though the average dust concentration may be optimal, there is no prior reason to expect that the minimum ignition energy should coincide with a uniform distribution. Finally, in *none* of the results cited, including those given here, were flow conditions in the spark gap known or controlled. Accordingly, one can only speculate as to whether even this lowest reported value of 2 mJ represents the "true minimum" for lycopodium in air.

To the aforementioned complications and contradictory requirements, one must add the following. The results are sensitive to electrode spacing for at least two reasons: (1) flame quenching occurs if the electrode spacing is too small, and (2) the conversion efficiency for stored electrical energy into effective spark energy is also a function of gap distance as shown in figures 12 and 13. The conversion efficiency also varies with circuit design and discharge duration (30, 43-44). For gas mixtures, where the absolute minimum ignition energies are low (10<sup>-3</sup> to 10 mJ), these problems are not so serious because conversion efficiencies are high and quenching diameters are small (5, 33, 42).

For dusts, these problems are severe because quenching diameters are larger and ignition energies are orders of magnitude higher, where conversion efficiencies are lower. For dust, there is also the inevitable limitation on the devolatilization rate, which tends to push the minimum toward higher dust concentrations, leading to further complications associated with the sharp cutoffs observed at high loadings caused by the physical-electrical interaction of the dust particles with the avalanche discharge. As was the case with the contradicting flow requirements, this physical-electrical interference is also unrelated to the intrinsic combustion properties of the dust.

The variables affecting the measurement of an absolute minimum in the electrical ignition energy for dust clouds have been studied by Eckhoff (13). He points out that while the concept of absolute minimum ignition energies for gases is a "sensible concept," the question is not so clear for dusts.

Examples of the complexities and contradictions are abundant for all dusts. Bartknecht (3) has summarized some of the more recent data for the "lowest minimum ignition energy." Curves similar to those shown in figure 26 characterize all dusts. The concentration at which the minima are observed is generally not identical to the optimum dust concentration which maximizes the explosion pressure or the rate of pressure rise. A significant particle size dependence is reported: The minimum energy increased an order of magnitude for polyethylene as the particle diameter increased from 30 to 100 μm. For the fine polyethylene the lowest minimum ignition energy was reported to be 30 to 40 mJ stored electrical energy. Bartknecht reports some preliminary tests on the influence of temperature for polyethylene which show an order of magnitude reduction in ignition energy for a 100° C increase in temperature. The data in figure 24 show a factor of 2 reduction per 100° C increase in temperature at a polyethylene concentration of 500 g/m<sup>3</sup>. The data also show that the temperature coefficient varies with both concentration and temperature.

Bartknecht's coworker Glarner (17) has measured the temperature dependence for the minimum ignition energy of lycopodium. His measurements cover the temperature range from 25° to 200° C, and he observed a reduction in the minimum ignition energy from 2 to 0.2 mJ over that temperature range. The reduction by a factor of 10 occurred at a lycopodium concentration of about 1,000 to 1,250 g/m<sup>3</sup>. The data in figure 19 show only a factor of 2 reduction over that same temperature range at a dust concentration of 260 g/m<sup>3</sup>. The coal dust data, however, shown in figure 16 do show that factor of 10 reduction at a coal dust concentration of 400 g/m<sup>3</sup>. Clearly the temperature coefficients are sensitive to both the dust concentration and the turbulence level. Nevertheless, the maximum observed reduction of about an order of magnitude in ignition energy between 25° and 200° C is comparable to what is observed for homogeneous mixtures of hydrocarbons in air under static conditions (17).

Swett (43-44) and Ballal and Lefebvre (2) have demonstrated beyond doubt that ignition energies for gases increase with increasing velocity and increasing turbulence intensity. Normally, increasing the time delay between dust dispersion and ignition would be expected to reduce turbulence levels. Glarner (17) has shown that the minimum spark energy and the dust concentration at which that minimum occurs are very sensitive to the delay time before ignition. Longer delay times correspond to reduced turbulence levels, which lead to a marked reduction in spark ignition energy requirements.

What meaning is there to the measurement of some minimum ignition energy stored in an external circuit in view of (1) the difficulties involved in measuring or controlling the flow and turbulence levels present during the dispersion of a dust cloud, (2) the sensitivity of the data to electrode geometry and circuit characteristics that are not standardized, (3) the generally unmeasured conversion efficiency of stored circuit energy into effective spark energy, (4) the dependence of the data on dust concentration, and (5) a temperature

sensitivity that is dependent on both dust concentration and the nature of the dust? So many uncontrolled factors influence the measurement that it is really very difficult to apply the result to any practical situation. Even if one of those factors, the dust concentration at which the minimum energy occurs, is also specified, the problem still seems intractable. Even if one measures the effective spark energy, as was done here, and then specifies the ignition energy that can barely generate a point of tangency to the room temperature isotherm, how representative is the result? While the room temperature minima for Pittsburgh coal and lycopodium appear to be fairly representative, polyethylene is a glaring example of unrepresentative behavior. Its minimum ignition energy at room temperature is entirely unrepresentative of its ignitability behavior between 115° and 395° C.

By contrast note how representative the minimum AIT's are of the entire shape of their respective thermal autoignition curves. For lycopodium, the entire lean-limit contour is predictable from the one datum point that represents the lean limit at room temperature. One expects that the Burgess-Wheeler law is similarly valid for coal dust. The melting behavior of polyethylene would probably complicate its lean-limit behavior above 115° C, but that remains to be determined by future experiments.

Summarized in table 2 are the lean-limit concentrations, the minimum AIT's, and room temperature minimum spark energies for all three of the dusts studied. In terms of either the lean limit of flammability or the minimum AIT, polyethylene is the most hazardous, lycopodium is intermediate, and coal dust has the lowest ranking. That order is also consistent with their respective volatile heating values. For spark ignitability, Pittsburgh coal is again the least hazardous and lycopodium and polyethylene are about equal, with lycopodium having the lowest ignition energy in the 1.2-L furnace but polyethylene having the lowest energy in the 20-L chamber. However,

the same ignitability data in figure 19 when compared with figures 16 and 24 show clearly that one does not need to know the exact value of the absolute minimum ignition energy at room temperature in order to establish that lycopodium is the most easily ignitable dust in the 1.2-L furnace. Lycopodium has the lowest ignition energy for all thermodynamic states in the intermediate domain that are practically accessible. Accordingly, there are many other single ignition energy parameters that are even more representative of its electrical ignitability hazard than the room temperature minimum ignition energy. For coal, for example, the minimum ignition energy occurs at such a high concentration that one can question its relevance to conditions normally encountered. A more realistic parameter for coal might be the ignition energy at some "standard" concentration, such as twice the lean-limit concentration. The room temperature  $\epsilon_{eff}$  values in the 1.2-L furnace at those concentrations are approximately 0.15 J for lycopodium, 1.0 J for polyethylene, and 5 to 6 J for coal. The order of electrical ignitability is still the same based on that new parameter, but the absolute  $\epsilon_{eff}$  values are probably now more realistic representations of normal situations. In some industrial operations, such as drying, elevated temperatures near 100° C are used. The 100° C  $\epsilon_{eff}$  values at twice the lean limit concentrations are approximately 0.04 J for lycopodium, 0.15 J for polyethylene, and 2 J for coal. In other practical situations one may prefer to fix both temperature and dust concentration. For example, at 100° C and 300 g/m<sup>3</sup> the  $\epsilon_{eff}$  values are approximately 0.04, 0.04, and 1.4 J, respectively. Now the polyethylene is, under these operating conditions, as hazardous as lycopodium. There is a natural desire to find some single ignition energy parameter that will accurately represent the electrical ignitability hazard of a dust under all operating conditions. While this seems to be easy for the well-behaved cases such as lycopodium or coal, the behavior of polyethylene does not allow such a simple representation. These examples have clearly illustrated

the practical deficiencies in using the concept of a minimum ignition energy as it is traditionally used. It is clearly still important to be able to measure the electrical ignition probability of various dusts, but it is unlikely that any single parameter will suffice to quantify that probability in a realistic way. The entire set of ignitability curves such as those delineated in figures 16, 17, 19, 22, 24, and 25 will probably suffice to determine the relative electrical ignition hazard for any set of specified operating conditions; however, the task of relating those relative values to realistic ignition probabilities in the presence of circuitry or electrical equipment of any given design is still rather formidable.

TABLE 2. - Summary of measured flammability and ignitability parameters for the three dusts.

	Pitts- burgh coal	Lyco- podium	Poly- ethylene
Lean flammability limit.... g/m <sup>3</sup> ..	130	70	45
Minimum AIT..°C..	560	420	395
Minimum ignition energy <sup>1</sup> , mJ:			
1.2-L furnace:			
$\epsilon_{eff}$ .....	250	50	70
$E_i$ .....	1,080	90	120
20-L chamber:			
$\epsilon_{eff}$ .....	70	35	30
$E_i$ .....	310	170	140

<sup>1</sup> $\epsilon_{eff} = 2.5 V_o \Delta p$  is the effective spark energy, and  $E_i = 1/2 CE^2$  is the stored electrical energy on the capacitor.

#### REFINEMENT OF THE THEORY OF MINIMUM IGNITION ENERGIES FOR GASES

In this second part of the discussion and interpretation, consideration is given to a wider range of ignition energy measurement, and particularly to earlier Bureau of Mines data for gases (5, 33). Those data will be interpreted in the context of a refinement of the general theory, which is developed as follows. Note that the symbols used are defined in the appendix.

Consider an initially quiescent, pre-mixed combustible gas mixture within which is imbedded a potential source of electric power in the form of a spark gap between two electrodes. Electric energy stored in some external circuit can be deposited into the spark gap in the form of an electron-ion avalanche discharge. The discharge occurs when the high voltage applied between the electrodes generates an electric field of sufficient intensity to break down the gas mixture gap and to cause it to conduct. It is assumed that the discharge energy is measurable directly or that one can show that some known fraction of the stored electrical energy is deposited into the conducting gap during the time of the electrical discharge. The important physical processes involved are initially considered in spherical symmetry, and the minimum *power* required to initiate spherical flame propagation is estimated as follows.

In several earlier studies (21, 23-24), the concept of limit burning velocities was developed and used to formulate a quantitative theory of flammability limits. The concept was developed by considering the balance between the rate of thermal energy generation in an adiabatic or ideal propagating flame front and the rate of energy loss from competing processes that dissipate power from the combustion wave. It was shown that the process responsible for the normal flammability limits, as conventionally measured, was the buoyancy-induced dissipative flows that result from natural convection. That dissipative process was characterized by a certain limit burning velocity  $(S_u)_a$ . Flame propagation was possible only for those mixtures whose ideal burning velocities exceeded that limit velocity. For horizontal flame propagation, the limit velocity was given by

$$(S_u)_a = [2\alpha g \rho_b / \rho_u]^{1/3}. \quad (26)$$

That minimum burning velocity corresponds to a minimum combustion source power density of  $(S_u)_a c \rho [(T_b)_\ell - T_u]$ . It should be noted that although the

details of the geometry for the buoyancy-induced flow field are not considered here, the effect of buoyancy on the combustion process is nevertheless included implicitly in  $(S_u)_a$ . Buoyancy-induced flows control the magnitude of  $(S_u)_a$  through the  $g$ -dependence and density ratio dependence,  $\rho_u / \rho_b$ , of equation 26.

To initiate flame propagation in the presence of the buoyancy-induced dissipative flows, the minimum source power density  $(S_u)_a c \rho [(T_b)_\ell - T_u]$  must be applied over some minimum ignition area. The minimum ignition area is taken as the area that bounds a minimum ignition volume. That minimum volume is characterized by a minimum radius  $r_q$ , whose magnitude is given by

$$r_q = \frac{2\alpha}{(S_u)_{\uparrow_{\text{deat}}}} (\rho_u / \rho_b). \quad (27)$$

The radius  $r_q$  is the "quenching radius" and equation 27 adequately predicts measured quenching diameters for a wide variety of fuel-oxidizer combinations over a wide range of values for  $\alpha$  and  $(S_u)_{\uparrow_{\text{deat}}}$  (21). Equation 27 also adequately describes the flame stretch quenching process involved in divergent flame propagation from a point source (22). The minimum ignition volume characterized by the radius  $r_q$  contains a minimum ignition area of  $4\pi r_q^2$ . Multiplying the minimum ignition area by the minimum source power density gives the minimum steady-state *power* required to initiate flame propagation.

$$\begin{aligned} P_{\text{min}} &= 4\pi r_q^2 (S_u)_a c \rho [(T_b)_\ell - T_u] \\ &= 16\pi\alpha^2 c \rho_u (\rho_u / \rho_b)^2 [(T_b)_\ell - T_u] \\ &\quad (S_u)_a / (S_u)_{\uparrow_{\text{deat}}}^2. \end{aligned} \quad (28)$$

The quantity  $P_{\text{min}}$  is the minimum source power that must be supplied from the external source, in steady state, to initiate the combustion wave. It is implicit in this derivation that the initiating source is a "point source." In realistic terms the "point source" must have dimensions that are small or comparable to  $r_q$ . It is also implicitly assumed that if the

"point source" condition is satisfied, the initial temperature of the source volume when it reaches dimensions comparable to  $r_q$  will be at least equal to the limit flame temperature,  $(T_b)_l$ . If those conditions are satisfied, source power levels of  $P_{min}$  and above should be capable of initiating the combustion wave. Input power levels below  $P_{min}$  would be incapable of ignition because of the presence of competing dissipative processes. Those competing processes are buoyant convection and flame stretch. They dissipate power to the surroundings at such a rate that any ignition source level below  $P_{min}$  is incapable of igniting the mixture regardless of its duration. Those competing processes dissipate the input source power continuously to the unburned surroundings and prevent the minimum volume from achieving a self-sustaining activation condition when the input power is less than  $P_{min}$ .

The classic experiments on ignition of gases by electric sparks were initiated by Guest (19) and reported in detail by Blanc, Guest, von Elbe, and Lewis (5). For those measurements, however, it was not the minimum power that was measured, but rather the minimum energy,  $E_{min}$ . In the normal experimental procedure a certain energy,  $E$ , is deposited into the combustible mixture in a very short time interval. The deposited energy is judged to have ignited or failed to ignite the mixture by whether or not flame propagates to distances far beyond the ignition electrodes. The instantaneous power level is usually not controlled. Only the available energy stored in an external circuit is controlled. For energy storage on a capacitor, the electrical discharge energy is related to its power level by the equation

$$E = \int_0^{\tau} p(t) dt, \quad (29)$$

where the time integral is taken over the entire duration of the discharge. Thus energy and power level are related to one another through the time variable.

Now there are at least two characteristic time constants involved in the processes by which the spark energy initiates the combustion wave. The first

one is the duration of the discharge,  $\tau_d$ . It is the characteristic time interval during which the electrical energy stored in the external circuit ( $1/2 CE^2$ ) is deposited into the gas gap between the electrodes. The second characteristic time constant is the chemical kinetic induction time,  $\tau_i$ . It is the time interval required for the development of the incipient flame front within the activated volume or at the boundary between the minimum ignition volume and the surroundings.

In an electric circuit that is activated by the closure of a "normal switch," the duration of current flow, or the circuit time constant, is controlled by the conventional circuit parameters: resistance, capacitance, and inductance. However, for electrical discharges, the gap is not a normal switch. In an electric discharge, the gap itself is an integral part of the circuit and its impedance exerts a dominant role. If the gap acted as a "perfect" switch which generated an ideal step function in resistance (from infinite resistance to zero resistance in a zero time interval), then absolutely *none* of the stored energy would appear in the spark gap. It is the finite time dependence of the resistance of the gap that is responsible for the fact that any energy at all is deposited in the gap. It is the electrical hysteresis properties of the gas mixture between the gap electrodes that cause it to act as a switch which initiates the transfer of energy from the external circuit to the gas. Initially the gap is a nearly perfect insulator until a critical field strength is reached. At the critical field strength, breakdown occurs; that is, the composition of the gas mixture in the gap and its electrical properties change drastically. An electron-ion avalanche process is initiated which results eventually in a reduction in the resistance of the gas mixture by many orders of magnitude. It is the time dependence of that dynamic spark gap impedance that controls the energy deposition rate. The available evidence indicates that only that fraction of the circuit energy that flows during the early stages of gas breakdown or current initiation can be

deposited at a high temperature into the gas gap (38). It is only during the early, higher impedance stages of the process that energy is most efficiently deposited into the gap. Once an ionization channel or plasma is well established in the gap, its impedance is reduced and the residual energy that may still be stored in the external circuit does not appear as efficiently in the gas. More of the residual energy stored later in the process is dissipated in the external circuit elements rather than in the air gap.

The detailed dynamics of the initiation process in such a time-dependent discharge are still apparently not well understood. By recording the pressure versus time trace in a constant-volume chamber within which a spark was discharged, Odgers and Coban (41) were able to follow the energy release in the gas of the gap. They concluded that the rise time for the pressure, and hence for the energy deposition rate, was less than 0.5 ms for their circuit. Maly and Vogel (38) characterize ignition sparks by three sequential processes or modes: an initial breakdown phase of short duration ( $10^{-4}$  ms), followed by an arc phase which ends after 0.01 ms, followed by a glow discharge which ends after about 1 ms. The efficiency of deposition of energy into the plasma of the gap declines more or less continuously in going from breakdown to glow as the gap resistance diminishes. Now the second characteristic time constant involved in the process of transition from electrical discharge to flame kernel is the chemical kinetic induction time,  $\tau_f$ . It is the time required for the development of an incipient flame front at the boundary of the minimum ignition volume.

The most careful direct study of the dynamics of the spark ignition process during this induction time prior to the establishment of a combustion wave at the boundary of an incipient flame kernel was that reported by Litchfield (36). His data for the chronology and topography of the ignition kernel during its formative stages provide a realistic picture of the

physical processes involved in the development of the incipient flame. He measured the time required for the "clear appearance of the flame." Using Schlieren techniques, his measured value at 0.1 atm for 8.5 pct methane in air was 1 ms. That value was consistent with the data of Lintin and Wooding (35), who reported an induction time of 0.1 ms at atmospheric pressure. Those values are also consistent with the recent measurements of Kono, Kumagai, and Sakai (30). Their measured values were also in agreement with their calculated values and were in the range of  $\tau_f \approx 0.1$  to 0.2 ms.

There are thus two important time constants involved,  $\tau_d$  and  $\tau_f$ , the former characterizing the rate of electrical energy input from the ignition source and the latter characterizing the rate of generation of chemical energy within the minimum ignition volume. The ignition process begins with the transfer of that electrical energy into chemical energy. In a sense, these time constants characterize the resistances or impedances of the two systems. Energy transfer is most efficient between systems when their impedances are matched. Thus one might expect that the most efficient transfer of energy from the electrical spark to the incipient flame would occur when the two time constants were matched; that is, when  $\tau_d \approx \tau_f$ . It is clear that if the spark duration is too long, such that  $\tau_d \gg \tau_f$ , spark energy will be delivered too slowly and will be dissipated. The energy integral in equation 29 would then be limited to a time interval of  $\tau_f$ , and spark energy delivered over any longer time interval would be dissipated to the surroundings, into gas volumes that are much larger than the minimum ignition volume. In that case, the power level for such an excessively long duration spark would be too low to initiate the combustion wave even if the total energy exceeded the minimum. Thus, even though the total spark energy would be given by

$$\epsilon_{\text{spark}} = \int_0^{\tau_d} p(t)dt,$$

where the total integral includes the entire spark duration,

the available or effective energy for ignition is  $\epsilon_{\text{eff}} = \int_0^{\tau_i} p(t) dt$ , and its duration is limited to the flame induction time,  $\tau_i$ .

But what harm is there in the opposite case, which is the usual one? If the spark duration is very short, then  $\tau_d \ll \tau_i$  and the energy is easily deposited before it can be lost to the surrounding volumes by natural convection and flame stretch. For such a short-duration spark, one would still have to wait for the time  $\tau_i$  before the flame would appear. But what harm is there so long as the energy remains in the ignition volume until the flame appears? The problem is that other loss processes are involved such as shock wave propagation and radiation. For a given energy of deposition, these additional loss processes increase with decreasing spark duration.

Thus long-duration sparks with  $\tau_d > \tau_i$  give increasing convective and flame stretch losses, whereas short-duration sparks with  $\tau_d < \tau_i$  result in increasing shock wave and radiation losses. It is not surprising, therefore, that in experiments in which the spark duration was varied, Kono, Kumagai, and Sakai (30) found a "well defined" optimum duration at which the ignition energy was minimized. That duration for propane-air mixtures was from 0.05 to 0.3 ms, in agreement with earlier measurements reported by Swett (43) and with the result of observations by Eckhoff and Enstad for dusts (14). Those optimum spark durations are comparable to the aforementioned independently measured values for  $\tau_i$ , observed by Litchfield (36) and Lintin and Wooding (35). They thus tend to confirm the expectation that the most efficient transfer of energy from the electric spark to the incipient flame occurs when the two time constants are matched; that is, when  $\tau_d \approx \tau_i$ .

With these considerations in mind, the most prudent approach would seem to require that the time constant involved in relating energy to power be considered

initially as a variable,  $\tau$ . Thus one sets

$$E_{\text{min}} = P_{\text{min}} \tau, \quad (30)$$

and substituting both forms of equation 28 into 30 one obtains first

$$E_{\text{min}} = \pi (S_u)_a c \rho_u [(T_b)_\ell - T_u] \tau d_q^2 \quad (31)$$

in terms of the quenching diameter,  $d_q$ . Or, in terms of the ideal burning velocity  $(S_u)_{\text{ideal}}$ , the minimum ignition energy becomes

$$E_{\text{min}} = 16\pi (S_u)_a c \rho_u (\rho_u/\rho_b)^2 [(T_b)_\ell - T_u] \tau \frac{\alpha^2}{(S_u)^2_{\text{ideal}}}. \quad (32)$$

The predictions of equation 31 are compared with the data in figure 27. Clearly, the empirical  $d_q^2$  dependence discovered by Lewis and von Elbe for hydrocarbon-oxygen-nitrogen mixtures is in excellent agreement with the prediction of equation 31. The data reproduced in figure 27 show that  $E_{\text{min}}$  correlates with  $d_q^2$  over a four-order-of-magnitude range in  $E_{\text{min}}$ .

For a more quantitative comparison one sets  $(S_u)_a$ , the horizontal limit burning velocity for quenching by natural convection, equal to its normal value of 6 cm/s (21, 23) and lets  $c = 0.30 \text{ cal g}^{-1} \text{ K}^{-1}$ ,  $\rho_u = 1.2 \times 10^{-3} \text{ g/cm}^3$ ,  $(T_b)_\ell = 1500 \text{ K}$ , and  $T_u = 300 \text{ K}$ . The result is

$$E_{\text{min}} (\text{mJ}) = 34 \tau (\text{ms}) d_q^2 (\text{cm}^2). \quad (33)$$

As the theoretical line in figure 27 shows, quantitative agreement between equation 33 and the data is obtained for  $\tau \approx 0.18 \text{ ms}$ .

That value of  $\tau$  is in the range of the values independently measured by Litchfield (36) and Lintin and Wooding (35) for the "clear appearance of flame." That value of 0.18 ms is also in the mid-range of the values reported by Kono, Kumagai, and Sakai (30) for the optimum

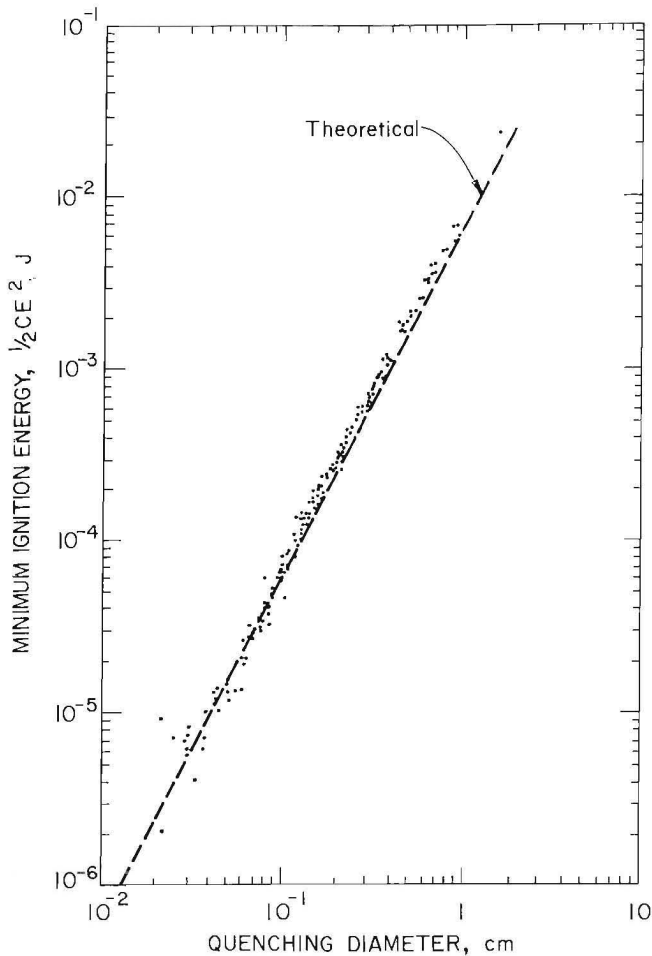


FIGURE 27. - Relationship between the minimum ignition energy and the quenching diameter for gases (5).

spark duration. Could the agreement between that  $\tau$ -value of 0.18 ms and the  $\tau_1$  values independently measured by the aforementioned researchers mean that the sparks used to obtain the energies reported in figure 27 were characterized by discharge durations that were all optimal? Is it plausible that in all those cases  $\tau_d \approx \tau_1$ ? That conclusion does not seem plausible if it is recalled that the data reported in figure 27 include a range of pressures from 0.1 to 2.5 atm, a range of oxygen contents from air to pure oxygen, and a broad range of equivalence ratios. Rather, it is more likely that the spark duration  $\tau_d$ 's were all much shorter than the  $\tau_1$ 's, but that their peak power levels were always small enough so that acoustic and radiant energy losses from the minimum ignition volume were insignificant fractions of the

spark energy deposited in the gap (14). If that is the case, what meaning is there then to the constancy of the  $\tau$ -value obtained from the data fit to equation 33? What is the physical significance to the absolute magnitude of 0.18 ms for that  $\tau$ -value?

The temptation is very strong to simply associate that  $\tau$ -value with  $\tau_1$ , the induction time for the establishment of an incipient flame front at the boundary of the minimum ignition volume. However, is it plausible to expect a constant  $\tau_1$ -value for all the mixtures represented by the data in figure 27? After all, they include a range of pressures from 0.1 to 2.5 atm, four different fuels (methane, ethane, propane, and hydrogen), a range of oxygen contents from air to pure oxygen, and a range of stoichiometries from lean to rich. The combustion energy densities and kinetic rates would vary markedly for such mixtures. It should be remembered, however, that while minimum energy densities for initiation vary markedly, the minimum volumes that are to be activated also vary but in inverse proportion to those energy densities. Similarly, although intrinsic burning velocities for those cases vary markedly, the "travel distance" for the incipient flame front is, in effect, the quenching radius  $r_q$ , and that radius also scales in inverse proportion to the burning velocity (equation 27). Thus it may be plausible to expect an invariant  $\tau_1$ -value even over such a wide range of experimental conditions.

During the incipient stage of kernel development there are *two* sources of energy available to the developing kernel. The first is the electrical energy deposited in the spark channel volume; the second is the energy being released by the combustion process within that same volume. The former, which is the quantity that is measured as the minimum ignition energy, only supplements the latter so that the higher the combustion energy in the minimum volume, the lower the required ignition energy. Although it is only the former that is measured experimentally when a flame is produced, the  $\tau_1$  value should be sensitive to *both*. Since both energies are involved in the

incipient stages of flame propagation and they are both spatially averaged over minimum volumes that are self-adjusting for various pressures, oxygen contents, fuels, and stoichiometries, it is not unreasonable to expect that the sum of those two energy densities would tend to

be invariant. As a result, the induction time for the transition from spark initiation within the quenching radius to independent propagation to just beyond  $r_q$  could reflect that constant total energy density and could also tend to be invariant.

#### CONCLUSIONS

The electrical ignition hazard for fuels has been traditionally specified in terms of their minimum ignition energies. For gases, the measurements are relatively simple and the results are in reasonable agreement with the established combustion theory (33). The measurements are complicated for dusts because the lowest ignition energies are obtained for a quiescent system, but the high dust concentrations at which the minima occur require turbulence for dispersion. Therefore, the true absolute minimum ignition energies may probably never be measured for dust clouds. However, the relative minimum ignition energies for various dusts can be measured, and these provide an estimate of the relative electrical ignition hazard for the various dusts. The minimum ignition energies for dusts are apparatus dependent as shown in this report, but the relative order of ignitability for different dusts can be useful in a hazard evaluation.

It is important to realize that a difference in minimum ignition energies of a factor of 2 may not be significant. Perhaps only if the minimum ignition energies of two dusts differ by almost an order of magnitude or more, can the one

dust be considered less hazardous electrically than the other. This can be seen in the minimum spark ignition data in this report (table 2). The minimum ignition energy value for lycopodium was slightly less than that for polyethylene in the 1.2-L furnace at room temperature but slightly higher than that for polyethylene in the 20-L chamber. The final conclusion is that these two dusts are about equal in electrical ignition hazard at room temperature. Pittsburgh coal dust, however, is more difficult to ignite than either lycopodium or polyethylene in either apparatus and is therefore less hazardous electrically.

The temperature coefficients for the electrical ignitability were also measured at various concentrations. The generalization that most dusts are more easily spark ignitable at elevated temperatures than at room temperatures is confirmed for the three dusts with the exception of polyethylene above 100° C. Its melting behavior causes a reversal of that normal trend. The temperature coefficient for the spark ignition energy is sensitive to both the type of dust and its concentration.

#### REFERENCES

1. American Society for Testing and Materials. Standard Test Method for Proximate Analysis of Coal and Coke, D3172-73; Standard Test Method for Ultimate Analysis of Coal and Coke, D3176-74; Standard Test Method for Gross Calorific Value of Solid Fuel by the Isothermal-Jacket Bomb Calorimeter, D3286-82. Sections in 1983 Annual Book of ASTM Standards, v. 05.05, Gaseous Fuels; Coal and Coke. Philadelphia, PA, 1983, pp. 394-439.
2. Ballal, D. R., and A. H. Lefebvre. The Influence of Flow Parameters on Minimum Ignition Energy and Quenching Distance. Paper in Fifteenth Symposium (International) on Combustion (Tokyo, Japan, Aug. 25-31, 1974). Combustion Inst., Pittsburgh, PA, 1975, pp. 1473-1481.
3. Bartknecht, W. Explosions. Springer, 1981, pp. 44-48.
4. Berg, R. H. Electronic Size Analysis of Subsieve Particles by Flowing

Through a Small Liquid Resistor. ASTM Pub. 234, 1959, pp. 245-255.

5. Blanc, M. V., P. G. Guest, G. Von Elbe, and B. Lewis. Ignition of Explosive Gas Mixtures by Electric Sparks. Paper in Third Symposium on Combustion and Flame and Explosion Phenomena. (Madison, WI, Sept. 7-11, 1948), Williams and Wilkins, 1949, pp. 363-367.

6. Burgess, D., and M. Hertzberg. The Flammability Limits of Lean Fuel-Air Mixtures. Thermochemical and Kinetic Criteria for Explosion Hazards. ISA Trans., v. 14, No. 2, 1975, p. 129.

7. Burgess, M. J., and R. V. Wheeler. Lower Limit of Inflammation of Mixtures of Paraffin Hydrocarbons With Air. J. Chem. Soc., v. 99, 1911, p. 2013.

8. Cashdollar, K. L., I. Liebman, and R. S. Conti. Three Bureau of Mines Optical Dust Probes. BuMines RI 8542, 1981, 26 pp.

9. Conti, R. S., K. L. Cashdollar, M. Hertzberg, and I. Liebman. Thermal and Electrical Ignitability of Dust Clouds. BuMines RI 8798, 1983, 40 pp.

10. Conti, R. S., K. L. Cashdollar, and I. Liebman. Improved Optical Dust Probe for Monitoring Dust Explosions. Rev. Sci. Instr., v. 53, 1982, pp. 311-313.

11. Coward, H. F., and G. W. Jones. Limits of Flammability of Gases and Vapors. BuMines B 503, 1952, 155 pp.

12. Dorsett, H. G., Jr., M. Jacobson, J. Nagy, and R. P. Williams. Laboratory Equipment and Test Procedures for Evaluating Explosibility of Dusts. BuMines RI 5624, 1960, 21 pp.

13. Eckhoff, R. K. Towards Absolute Minimum Ignition Energies For Dust Clouds? Combustion and Flame, v. 24, 1975, pp. 53-64.

14. Eckhoff, R. K., and G. Enstad. Why Are "Long" Electric Sparks More Effective Dust Explosion Initiators Than "Short" Ones? Combustion and Flame, v. 27, 1976, p. 129.

15. Eggleston, L. A., and A. J. Pryor. The Limits of Dust Explosibility. Fire Technol., v. 3, 1967, pp. 77-89.

16. Gibbs, J. W. On the Equilibrium of Heterogeneous Substances. Trans. CT

Acad. Sci., 1876 (also available in J. W. Gibbs, Collected Works. Longmans, Green & Co., New York, 1928, pp. 63, 96.)

17. Glarner, T. Temperatureinfluss auf das Explosions und Zündverhalten brennbarer Staube (Influence of Initial Temperature on Explosion and Ignition Behavior of Combustible Dusts). Doctoral Thesis No. 7350, Eidgenössischen Technischen Hochschule, Zurich, Switzerland, March 9, 1983, 218 pp.

18. Godbert, A. L., and H. P. Greenwald. Laboratory Studies of the Inflammability of Coal Dusts: Effect of Fineness of Coal and Inert Dusts on the Inflammability of Coal Dusts. BuMines B 389, 1935, 29 pp.

19. Guest, P. G. Apparatus for Determining the Minimum Energies for Electric Spark Ignition of Flammable Gases and Vapors. BuMines RI 3753, 1944, 16 pp.

20. Hertzberg, M. The Flammability Limits of Gases, Vapors and Dusts: Theory and Experiment. Paper in Fuel-Air Explosions, ed. by J. H. S. Lee and C. M. Guirao (Proc. Int. Conf. on Fuel-Air Explosions, McGill Univ., Montreal, Canada, Nov. 4-6, 1981). Univ. Waterloo Press, Waterloo, Canada 1982, Study No. 16, pp. 3-48.

21. \_\_\_\_\_. The Theory of Flammability Limits. Conductive-Convective Wall Losses and Thermal Quenching. BuMines RI 8469, 1980, 25 pp.

22. \_\_\_\_\_. The Theory of Flammability Limits. Flow Gradient Effects and Flame Stretch. BuMines RI 8865, 1984, 36 pp.

23. \_\_\_\_\_. The Theory of Flammability Limits. Natural Convection. BuMines RI 8127, 1976, 15 pp.

24. \_\_\_\_\_. The Theory of Flammability Limits. Radiative Losses and Selective Diffusional Demixing. BuMines RI 8607, 1982, 38 pp.

25. Hertzberg, M., K. L. Cashdollar, and C. P. Lazzara. The Limits of Flammability of Pulverized Coals and Other Dusts. Paper in Eighteenth Symposium (International) on Combustion (Waterloo, Canada, Aug. 17-22, 1980). Combustion Inst., Pittsburgh, PA, 1981, pp. 717-729.

26. Hertzberg, M., K. L. Cashdollar, D. L. Ng, and R. S. Conti. Domains of Flammability and Thermal Ignitability for Pulverized Coals and Other Dusts. Particle Size Dependences and Microscopic Residue Analyses. Paper in Nineteenth Symposium (International) on Combustion (Haifa, Israel, Aug. 8-13, 1982). Combustion Inst., Pittsburgh, PA, 1983, pp. 1169-1180.
27. Hertzberg, M., K. L. Cashdollar, and J. J. Opferman. The Flammability of Coal Dust-Air Mixtures. Lean Limits, Flame Temperatures, Ignition Energies, and Particle Size-Effects. BuMines RI 8360, 1979, 70 pp.
28. Jacobson, M., J. Nagy, and A. R. Cooper. Explosibility of Dusts Used in the Plastics Industry. BuMines RI 5971, 1962, 30 pp.
29. Jacobson, M., J. Nagy, A. R. Cooper, and F. J. Ball. Explosibility of Agricultural Dusts. BuMines RI 5753, 1961, 23 pp.
30. Kono, M., S. Kumagai, and T. Sakai. The Optimum Condition for Ignition of Gases by Composite Sparks. Paper in Sixteenth Symposium (International) on Combustion (Cambridge, MA, Aug. 15-20, 1976). Combustion Inst., Pittsburgh, PA, 1977, pp. 757-766.
31. Kubala, T. A., F. J. Perzak, and E. L. Litchfield. Electric Ignition of Lycopodium Powder in a Modified Hartmann Apparatus. BuMines RI 8600, 1981, 9 pp.
32. LeChatelier, H., and O. Boudouard. Sur les limites d'inflammabilité des mélanges gazeux (On the Limits of Inflammability of Gaseous Mixtures). Bull. Soc. Chim. (Paris), v. 19, 1898, p. 483.
33. Lewis, B., and G. von Elbe. Combustion, Flames and Explosions of Gases. Academic, 2d ed., 1961, 731 pp.
34. Liebman, I., R. S. Conti, and K. L. Cashdollar. Dust Cloud Concentration Probe. Rev. Sci. Instr., v. 48, 1977, pp. 1314-1316.
35. Lintin, D. R., and E. R. Wooding. Investigation of the Ignition of a Gas by an Electric Spark. Brit. J. Appl. Phys., v. 10, 1959, pp. 159-166.
36. Litchfield, E. L. Chronology and Topography of Sparks at Minimum Energy for Ignition. Combustion and Flame, v. 5, 1961, p. 235-241.
37. \_\_\_\_\_. Minimum Ignition-Energy Concept and Its Application to Safety Engineering. BuMines RI 5671, 1959, 10 pp.
38. Maly, R., and M. Vogel. Initiation and Propagation of Flame Fronts in Lean CH<sub>4</sub>-Air Mixtures by the Three Modes of the Ignition Spark. Paper in Seventeenth Symposium (International) on Combustion (Leeds, England, Aug. 20-25, 1978). Combustion Inst., Pittsburgh, PA, 1979, pp. 821-831.
39. Nagy, J., H. G. Dorsett Jr., and A. R. Cooper. Explosibility of Carbonaceous Dusts. BuMines RI 6597, 1965, 30 pp.
40. National Fire Protection Association (Boston, MA). Fire Protection Handbook. 14th ed., 1976, pp. 3-106 - 3-118.
41. Odgers, J., and A. Coban. The Energy Release to Static Gas From a 12-Joule High Energy Ignition System. Pres. at Gas Turbine Conference and Products Show, Philadelphia, PA, Mar. 27-31, 1977; Paper 77-GT-18, available from American Society of Mechanical Engineers, New York, 13 pp.
42. Roth W., P. G. Guest, G. von Elbe, and B. Lewis. Heat Generation by Electric Sparks and Rate of Heat Loss to Spark Electrodes. J. Chem. Phys., v. 19, 1951, p. 1530.
43. Swett, C. C., Jr. Effect of Gas Stream Parameters on the Energy and Power Dissipated in a Spark and on Ignition. Paper in Third Symposium on Combustion and Flame and Explosions Phenomena (Madison, WI, Sept. 7-11, 1948). Williams and Wilkins, 1949, pp. 353-361.
44. \_\_\_\_\_. Spark Ignition of Flowing Gases Using Long Duration Discharges. Paper in Sixth Symposium (International) on Combustion (New Haven, CT, Aug. 19-24, 1956). Reinhold, 1957, pp. 523-532.
45. U.S. Bureau of Mines. Methods of Analyzing and Testing Coal and Coke. B 638, 1967, 82 pp.

46. Warnatz, J. The Structure of Laminar Alkane-, Alkene-, and Acetylene Flames. Paper in Eighteenth Symposium (International) on Combustion (Waterloo, Canada, Aug. 17-22, 1980). Combustion Inst., Pittsburgh, PA, 1981, pp. 369-384.

47. Zabetakis, M. G. Flammability Characteristics of Combustible Gases and Vapors. BuMines B 627, 1965, 121 pp.

48. Zabetakis, M. G., A. L. Furno, and G. W. Jones. Minimum Spontaneous

Ignition Temperatures of Combustibles in Air. Ind. and Eng. Chem., v. 46, 1954, pp. 2173-2178.

49. Zabetakis, M. G., S. Lambiris, and G. S. Scott. Flame Temperatures of Limit Mixtures. Paper in Seventh Symposium (International) on Combustion (London and Oxford, England, Aug. 28-Sept. 3, 1958). Butterworths, 1959, pp. 484-487.

## APPENDIX.--SYMBOLS AND NOMENCLATURE

AIT	Autoignition temperature.	$P_{min}$	Minimum steady-state power for ignition.
c	Heat capacity.	$p(t)$	Instantaneous power of spark discharge.
$c(T)$	Heat capacity at temperature T.	$Pr(expl)$	Explosion probability.
$\bar{c}$	Effective heat capacity.	$Pr(f)$	Probability of the existence of a flammable volume.
C	Capacitance.	$Pr(i)$	Ignition probability.
$C_T, C_{25}$	Lean flammability limits (in mass concentration) at temperature T and 25° C, respectively.	$Pr(i, spark)$	Probability of spark ignition.
$d_q$	Quenching diameter.	$Pr(i, t)$	Probability of thermal auto ignition.
$\bar{D}_s$	Surface-area-weighted mean particle diameter.	$r_q$	Radius of minimum ignition volume or quenching radius.
$\bar{D}_w$	Mass- or volume-weighted mean particle diameter.	R	Gas constant.
E	Electrical potential or voltage.	$(S_u)_a$	Limit burning velocity.
$E_i$	Stored electrical energy of external circuit for spark.	$(S_u)_{ideal}$	Ideal laminar burning velocity.
$E_{min}$	Minimum ignition energy.	t	Time.
g	Gravitational acceleration.	T	Temperature.
H:C	Hydrogen-to-carbon ratio.	$T_o$	Ambient temperature.
$\Delta H_c$	Heat of combustion.	$T_f$	Final temperature of spark discharge channel.
$L_T, L_{25}$	Lean flammability limits in volume percent at temperature T and 25° C, respectively.	$(T_b)_l$	Limit flame temperature.
M	Molecular weight.	$T_u$	Temperature of unburned gases.
p	Pressure.	$v_i, v_f$	Initial and final volumes of spark discharge channel.
$P_o$	Ambient pressure.	$\Delta v$	Change in volume of spark discharge channel.
$\Delta p$	Pressure rise.		

$V_o$	Chamber volume.	$\epsilon_{\text{spark}}$	Total spark energy.
$(V_u)_i, (V_u)_f$	Initial and final unaffected volumes of chamber (i.e., total volume minus spark channel volume).	$\nu$	Degrees of freedom in the motion of an atomic or molecular system.
$\Delta V_u$	Change in the unaffected volume of chamber.	$\rho_T, \rho_{25}$	Density of fuel at temperature T and 25° C, respectively.
w	Work done by spark in raising pressure of chamber.	$\rho_u, \rho_b$	Density of unburned and burned gases, respectively.
$x_j$	Mol fractions of components in mixture.	$\rho$	Density of flammable mixture.
$\alpha$	Effective diffusivity.	$\tau$	Time.
$\beta$	General temperature coefficient for any fuel.	$\tau_d$	Length of time of spark discharge.
$\gamma$	Temperature coefficient for paraffin hydrocarbons.	$\tau_i$	Chemical kinetic induction time.
$\epsilon_{\text{eff}}$	Effective spark energy, equal to $2.5 V_o \Delta p$ .		